Hydrodynamic Simulation and Optimization of an Oil Skimmer

by

© An'ran Zhang

A Thesis submitted to the

School of Graduate Studies

in partial fulfillment of the requirements for the degree of

Master of Engineering

Faculty of Engineering and Applied Science

Memorial University of Newfoundland

October 2015

St. John's Newfoundland

ABSTRACT

Oil spills can cause severe environmental damage. The challenges of removing oil spills in the sea arise when a vessel is operated in heavy sea and current conditions. An oil skimmer has recently been developed by Extreme Spill Technology (EST) Inc. for automated oil recovery by using vacuum mechanism. This thesis discusses numerical and experimental results of the hydrodynamic performance of the oil recovery process conducted by the oil skimmer. The process of oil recovery by the vacuum mechanism is complicated and involves multi-phase and multi-scale moving interfaces, including oil, water, atmospheric air and attenuated compressible air on the top part of the vacuum tower, a moving interface of an oil slick, oil droplets and air bubbles of different scales. The recovery process was simplified into a three-phase flow problem involving oil, water and air and simulated using a Computational Fluid Dynamic (CFD) method. The volume of fluid (VOF) method was employed to capture the moving surfaces between the fluid phases. Numerical results were compared with the experimental data. The research was also extended to optimize the geometry of the tower along with the service speeds of the oil skimmer model for maximizing oil recovery.

During this research process, my work was to investigate the numerical simulation of the hydrodynamic performance of the oil skimmer model and to provide the optimized geometries and service speeds based on the results from CFD analysis. The verification experiments were also designed and completed. The successful numerical simulation

results for the oil skimmer with the optimized geometry will be beneficial for the field test in the future. The improvements can be made directly to the existing oil skimmer models.

ACKNOWLEDGEMENTS

I would like to take this opportunity to thank my supervisor Dr. Wei Qiu for his guidance throughout my research. I would like to thank our postdoctoral fellow Dr. Shaoyu Ni for his invaluable help in my work. Their suggestions and experiences did improve the efficiency of my research. I would like to thank Extreme Spill Technology Inc. for providing the prototype of the oil skimmer. I would like to thank the National Science and Engineering Research Council of Collaborative Research and Training Experience (NSERC CREATE) Research Program of Offshore Technology for the financial support.

I would like to thank all the technicians in the Hydraulic Lab, Memorial University, for helping me set up the experimental apparatus. I am grateful to the Ocean Engineering Research Center for providing the experimental equipment for my research studies.

I would like to thank my fellow students in the Advanced Marine Hydrodynamics Lab oratory for their encouragement and inspiration. I would also like to thank my family for their continued support. Without help from these people, this thesis would not have been possible.

Last but not the least, I would like to thank God who guides me through all difficulties in my life. I do know that He is always there when I need Him. Praise the grace of Jesus Christ.

Table of Contents

List of Tables

List of Figures

Nomenclature

B_{Tower}	beam of skimming tower, mm
C	the Courant number
d_{Air}	initial air layer thickness in tower, mm
d_{Oil}	initial oil layer thickness in tower, mm
d_{Water}	initial water layer thickness in tower, mm
d'_{Oil}	final oil layer thickness in tower, mm
d_0	equivalent diameter of an encapsulated drop, mm
d_r	horizontal diameter of an encapsulated drop, mm
d_z	vertical diameter of an encapsulated drop, mm
F_{Oil}	volume fraction of oil
F_{Water}	volume fraction of water
F_{Air}	volume fraction of air
F_n	Froude number
g	gravity, m/s^2
h_0	height of sloping deck, mm
h_{sta}	static pressure, Pa
h_{Oil}	height of oil layer, mm
h_{Water}	height of water layer, mm
k	turbulent kinetic energy, J/kg
L	ship length, mm

L_{Tower}	tower length, mm
n_{δ}	number of grids for the oil layer
n_{Tower}	number of grids for tower
n_{Total}	number of grids for computation domain
P_{atm}	atmospheric pressure, Pa
P_0	1 atmospheric pressure, Pa
q	discharge rate
Q_0	Fully skimmed oil per second
Q	skimmed oil per second
$Q_{Oil-inflow}$	oil inflow per second
R	gas constant, $Nm/kg^{-1}K^{-1}$
r_0	equivalent radius of an encapsulated drop, mm
r'	radius of inner gas bubble, mm
T	temperature, K
t	time, s
$u_i(i = 1,2,3)$	velocity components
U	velocity of an encapsulated drop, m/s
v	ship speed, m/s
V_{Oil}	skimmed volume of oil
V_{Tower}	volume of tower
V_{Total}	volume of computation domain
(x, y, z)	Cartesian coordinate

Δ	radius ratio of an encapsulated drop
Δt	time step, s
Δx	length interval, m
ϵ	turbulence dissipation rate, J/kgs
δ_{ij}	Kronecker delta
δ_{Oil}	oil thickness, mm
ϑ	deformation ratio of an encapsulated drop
μ_{Oil}	oil viscosity, mm^2/s
μ_t	eddy viscosity, mm^2/s
ρ_{Oil}	oil density, kg/m^3
ρ_{Water}	water density, kg/m^3
ρ_{Air}	air density, kg/m^3
σ	skimmed oil rate
ω	angular frequency, rad/s

Abbreviation

CFD	Computational Fluid Dynamic
EST	Extreme Spill Technology Inc.
PIV	Particle Image Velocimetry
RANS	Reynolds-Averaged Navier-Stokes equations
SOS	Seaway independent Oil Skimming system
UDF	User Defined Function
VOF	Volume of Fluid

Chapter 1

Introduction

Oil spills are always referred to the released liquid petroleum hydrocarbon into the environment, especially marine seas. The oil spills can be extremely harmful to the marine ecological environment. They can also cause various damages effects both onshore and offshore. In this case, the efficient and effective oil spills clean up methods will be in great demand. The current oil response techniques and devices are introduced in this chapter, including in-situ burning, chemical methods and mechanical methods. An innovative oil skimmer is also introduced, and the principle of oil recovery is described.

1.1 In-situ Burning Method for Oil Spills Clean Up

In-situ burning is regarded as an emergency oil spill response technique that involves the controlled ignition and burning of the oil at or near the spill site on the surface of the water. Mullin et al. (2003) summarized the merits and demerits of the application of in-situ burning method. They also concluded that the requirements and concerns to burn the oil, including the flame temperatures, slick thickness, and residue after burning, etc. Even if few actual cases of in-situ burning on open waters, this oil response tool has been gaining renewed interest due to its high recovery efficiency and minimal requirement of

specialized equipment. The paper especially indicated that in-situ burning could be potentially effective for a medium to very large scale of oil spill.

In-situ burning method for oil spill clean up has been investigated for decades by a wide variety of researchers numerically and experimentally. However, this method is always considered as the last resort to clean up the oil spill. Evans et al. (2001) described the guidelines developed by National Institute of Standard and Technology (NIST) that were to establish the burning oil system and to deal with the emergent oil response issues. They conducted the burning oil experiments from small scale to large scale at sea, and a commercial software, ALOFT, was employed to simulate the smoke plume trajectory after the oil spills burning. They also concluded that the hesitation to apply in-situ burning was mostly due to the unknown characteristics of smoke after burning. The method introduced Evans et al. (2001) has a reliable prediction of the downwind concentrations of the smoke particulate transported by wind-blown fire plumes.

During conducting of in-situ burning, the estimation of oil windows-of-opportunity is introduced when the most effective oil burning will occur. The term of time period windows-of-opportunity is defined as the period where oil response methods and technologies are the most effective, which was given by Nordvik et al. (2003). The estimation of time period windows-of-opportunity is the most essential matter for operating in-situ burning. It is pointless proceeding to in-situ burning if this method is not feasible. Therefore, they developed three important steps to estimate the time period to

maximize the oil burning effectiveness. In order to demonstrate their time estimation model, an oil spilled case that occurred on the Alaskan North Slope (ANS) was studied to estimate the time period which was employed to compare with the existing data. Buist (2003) also described the fundamentals that affected the time window-of-opportunity for in-situ burning of oil at sea. He included the requirements for ignition and sustained burning, along with the factors that can influence the quality of residue and oil burning efficiency. In addition, he mentioned that the oil response of in-situ burning might be the only oil removal option to be used in the ice-covered water.

There have a number of studies to prove that in-situ burning leads to greater recovery efficiency than that from other oil clean up methods. Buist et al. (1999) found that the oil removal efficiency for thick oil slicks could easily exceed 90%. They mentioned that the removed rates of 2000 m^3/h that can achieve with a fire are only of about 10,000 m^2 or a circle of about 100 m in diameter. However, there are certain concerns mainly focused on the negative effects from in-situ burning. Firstly, secondary fires from the residue of in situ burning that threatens human life, property and natural resources need to pay more attention. Secondly, the products that come from burning, primarily the smoke, are highly toxic and usually involve potential environmental problems and human-health effects.

1.2 Chemical Methods for Oil Spills Clean Up

To use chemical dispersants for oil spills clean up is another useful method under certain conditions. The most popular chemical material is dispersing agents, gelling agents and

biological agents. However, there are two major concerns associated with the application of dispersant, where one is effectiveness and the other is toxicity after dispersing in the water column. It is well known that the advantage of using dispersants is that can remove a great amount of oil from the water surface into the water column when the oil is diluted and dispersed, while the toxicity of dispersant can remain in the water at the same time. It can affect the wild life and the health of human being through the contaminated water. In addition, it can be expensive, complex and labor intensive operation for a large scale of oil spill.

Research to investigate chemical dispersants to clean up oil spills was started since 1960s. Dewling et al. (1980) described six effective types of chemical dispersants for mitigating the environmental effects resulting from oil spills. They also admitted that the use of chemical dispersants for eradicating visible oil might have severe impact on the aquatic environment and destroy the delicate balance of aquatic ecology which can result in the extinction of valuable species. However, Lessard et al. (2000) claimed that the dispersants used today could lead to lower overall environmental effects than other oil spill response techniques. The improved dispersant products with lower toxicity to marine life and more effective at dispersing heavy and weathered oil have been growing acceptance worldwide. They also mentioned that a new generation of dispersant developed by Exxon Mobile was demonstrated to be effective both in laboratory and field tests on the types of oil that previously was considered not dispersible.

Mechanical oil recovery method should been traditionally preferred as the oil spill response technique in Norway for the past decades, although the use of dispersant has been gaining interest according to Daling et al. (2002). They gave a detailed review on the dispersants applied in the various field trails in the recent years, as well as describing the basic information of modeling Oil Spill Contingency and Response (OSCAR) which was a tool for objective analysis of alternative spill response strategies. Reed (2004) et al. developed this model system in shallow coastal water by coupling three-dimensional oil spill and hydrodynamic models to map hydrocarbon concentration in the water column and on the sea floor by solving a function of time following dispersant application. Since the numerical model was centered on the shallow water, certain fractions of the released hydrocarbon were attached with bottom sediments. However, since the algorithms to model sediment interaction were hypothetic, experimental data were required to validate.

Chapman et al. (2007) reviewed the use of dispersants on spills which occurred from 1995 to 2005, during which there were few occasions to apply chemical dispersants to clean up oil spill in Europe. Even if the chemical dispersant products are getting less toxic, they emphasized that more field trails and advanced multidisciplinary scientific research for the application of dispersants were still necessary.

Diemand and Francis (2011) have researched the application of dispersants in the oilspills of the Gulf of Mexico occurred in 2010. They studied that the effectiveness and toxicity to apply COREXIT 9500 and 9527. They concluded that the chemically dispersed oil

would be less toxic than the physically dispersed oil. They also indicated that COREXIT 9527 has negative effects on development and fertilizaiton of sea urchin. Graham (2010) pointed out that the selection of dispersants would be varied within different countries. He also emphasized that the successful dispersant operation system would be necessary during the process.

1.3 Mechanical Methods for Oil Spills Clean Up

Mechanical method is always considered as the most common oil response technique, which includes a wide variety of oil-booms and skimmers. To use mechanical recovery operation can involve large carrier ships, temporary storage devices, skimming systems, pumping equipment, and disposal system. The mechanical recovery system will generate a great amount of oil and water mixture that requires various disposal methods, like landfill, recycling or incineration. However, employing mechanical method for oil spills clean up can be expensive and time wasting. The recovery efficiency is also a major concern, which is rarely over 20% according to Mullin (2003).

1.3.1 Oil Booms

Oil booms are also known as barriers that are used to confine oil slicks on the water surface, then to thicken the oil layer so that skimmers, vacuums or chemical dispersants can be applied more effectively. The use of oil booms is very common in the oil spill response for the past decades. However, the failure of oil booms can be seen in a few

conditions where oil booms cannot contain the oil successfully. In this case, the oil will escape underneath the oil boom due to hydrodynamic forces. Goodman et al. (1996) used Computational Fluid Dynamic (CFD) software accurately to simulate three boom failure cases that were drainage failure, droplet entrainment, and critical accumulation.

Since the oil boom is still the popular equipment to confine the oil spill, the efforts to increase the recovery effectiveness are being made. There are a variety of innovative oil boom system been developed recently. Wong et al. (2003) presented a flexible oil boom system that was concentrated on the ramp boom equipped with a number of flaps to adjust itself to non-uniform flow conditions. They also studied the performance of the flexible ramp impacted by various dimensionless parameters and length scales.

The numerical modelling of both oil booms and oil spills is also being required for increasing attention, which is able to numerically study the criteria, and to extend it for better design in the future. Muttin (2008) developed the numerical model to analyse oil booms to confine spilled oil in very calm seas, in which finite element method was employed. However, Violeau et al. (2007) indicated that finite element method of finite volume method might fail in simulating complex models, such as a two-phase turbulent flow with fluid structure interaction. In this case, they presented a numerical model of floating boom and oil spills with the application of the Smoothed Particle Hydrodynamics (SPH) Lagrangian numerical method. They also studied the typical oil boom failure by the numerical method. A steady open-channel flow and regular waves in a flume were

considered, while the surface tension forces in this model were neglected and three-dimensional case was not taken into account. Yang et al. (2013) also presented a numerical model by using SPH method to simulate oil booms with water-oil two-phase flows, complex free surfaces and deformable interfaces. They improved the SPH equations to obtain numerical stability, as well as enhanced boundary condition for accuracy and flexibility. Four major factors influencing the oil boom failure were investigated, while more laboratory experiments and more influencing factors were still highly required.

1.3.2 Oil Skimmer

There have been several types of mechanical oil skimmers developed to respond the oil spills. Oil skimmer is one of the most widely used oil spill response methods. Mechanical oil skimmers for oil collection in calm water have been researched by Leibovich (1977). There are three types of oil skimmers popular in practical application: (1) weir skimmers, (2) rotating disk skimmers, and (3) pumping or vacuum skimmers. Leibovich (1977) described that mechanical oil skimmers had apparent limitations when applied in rough seas since they were not flexible and robust. Keller et al. (2006) have worked to improve the efficiency of mechanical oil spill response equipment by optimizing the geometry of the olephilic skimmer recovery surface. They presented that the recovery efficiency was up to three times by installing the new surface pattern in the recovery system. Field tests were also conducted to study the relation between the operational variables and the oil spill recovery efficiency.

The application of mechanical oil skimmer can be a very time-consuming and expensive approach for a large scale of oil spills due to their low recovery rate. Mechanical oil recovery by using weir skimmers is one of the most important techniques in responding oil spills at sea. There are few studies on handling the unique hydrodynamic conditions concerning the flow of floating oil over weir skimmer, which was indicated by Hammoud (2006). He presented the improved performance of a weir skimmer by introducing a tangential water jet equipped inside the skimmer. A series of experiments were conducted to investigate the factors to influence the skimmer oil recovery rate, including water jet flow, oil viscosity, and oil film thickness.

There also has been a wide range of disk skimmers equipped in many commercial skimming systems according to Cormack (1983), Marcinowski (1976), and Thomas (1977). The application of rotating disk skimmer to combat oil spills is one of the most popular mechanical oil recovery method because of its capabilities to deal with various oil film thickness and oil viscosity. Christodoulou et al. (1990) presented a theoretical model for better understanding of the hydrodynamic performance of the rotating disk skimmer at low to moderate speeds, while this analytical model was limited to low Reynolds number. Turner (2000) et al. investigated the importance of various parameters for the rotating disk skimmer based on the theoretical study by Christodoulou et al. (1990). They also conducted a series of tests to enhance the oil recovery rate with the modified rotating disk skimmer.

Clauss et al. (2006) have developed a model of a Seaway independent Oil Skimming system (SOS) numerically and experimentally. The SOS was equipped with an oil recovery vessel. The Oil Skimming system can separate wave damping from the skimming process without using moving parts. They also presented that the oil recovery efficiency was up to 70% in random seas and was up to 87% in calm water. The application of CFD method was to analyze the oil recovery rate where the simulation involved a three-phase-flow in the oil skimmer conducted in a numerical wave tank. The geometry of the oil skimmer was evaluated and optimized by employing the model tests. Clauss et al. (2007) investigated the oil skimmer system under both water-air two-phase flow condition and water-oil-air three-phase flow condition. They also used CFD software to simulate the oil skimmer model and completed the validation for the three-phase flow with different scales. In addition, the model tests were conducted at different cruising speeds and at different sea states. The improved oil skimming system by Clauss et al. (2009) was more effective on rough seas. In order to prevent the oil spills from emulsification and weathering process, they developed their model with high transit velocities on recovering oil.

1.4 An Alternate Approach of Vacuum Oil Skimmer

An innovative oil skimmer has been recently developed by Extreme Spill Technology (EST) for automated oil recovery by installing a vacuum device in a vessel. This thesis is mainly focused on this renovated vacuumed oil skimmer. The initial tests in calm water

have shown that the prototype vessel is efficient in oil recovery. Note that the skimming vessel has a sloping deck in front of the skimming tower and a submerged deck below the tower. This feature can potentially benefit the oil recovery process. In addition, the sloping plane begins aft of the bow, not at the bow, which can avoid the oil to escape sideways when incoming waves hit the sloping plane and splash back. The catamaran prototype with a vacuum tower installed onboard, which was also presented by Qiu et al. (2013), is showed in Figure 1.1.

The principle of the oil recovery for the EST vacuum oil skimmer is quite simple and straight forward. Initially, the air pump on the top of the vacuum tower is turned on so that the air inside the tower is pumped out. Since the air pressure in the tower is lower than that in atmosphere, the fluid mixture of oil and water enters the tower to a certain height. While the vessel with the air pump off is advancing in oil slicks, the oil flows into the tower continuously along the sloping deck in front of the tower because the density of oil is lower than that of water. When the skimming tower is full of oil, the oil can be transferred to oil storage devices.

Although the principle of the vacuum mechanism for oil skimming is simple, the hydrodynamic aspects of the recovery process is rather complicated. It involves multi-phase and multi-scale moving interfaces, including oil, water, atmospheric air and attenuate compressible air on the top region of the tower, and moving interface of oil

slicks, oil droplets and air bubbles of different scale. To have a better understanding of the hydrodynamic performance of the oil skimmer is essential.

1.5 Review of Computational Fluid Dynamic method

CFD method has been widely applied to analyse the multi-phase flow problem in the past decades. Clauss et al. ((2006), (2007), and (2009)) used CFD software to simulate both the oil skimmer model and the full scale oil skimmer with varied sea states. Clauss et al. (2004) investigated the numerical model for calculating two-phase flow and three-phase flow around the oil skimmer with CFD method that were based on the coupling of the Reynolds Averaged Navier Stokes equations and a Volume of Fluid (VOF) method. The numerical results from their CFD models were also systematically validated.

The VOF method was employed to capture the moving surfaces between the fluid phases. Noh and Woodward (1976) first developed the VOF method which can be numerically applied to trace and locate the free surface or fluid-fluid interface in the computational domain. The first publication employing the VOF method in computational fluid dynamics was from Hirt and Nichols (1981). They presented a few examples employing the VOF method to track the free surface that indicated the VOF method could work extremely well for a wide range of complicated problems. Hyman (1984) described the implementation of VOF method in tracking free surface, which can simply and accurately account for the interactions of many different smoothly varying interfaces. He also

mentioned that the volume fractions would be updated during the calculation where the interface position could be reconstructed cell wise on each time step.

In this work, the recovery process was simplified into a three-phase flow problem involving oil, water and air in the numerical simulation. The VOF method was applied to capture free surfaces and the interface between fluid-fluid phases. A commercial Computational Fluid Dynamic software, Star-CCM+, was adopted for the simulations. Star-CCM+ is a CFD software program which has a set of features to deal with complex hydrodynamic problems. The use of CFD software for hydrodynamic simulations of an oil skimmer can also predict the potential limitations of oil skimming systems with multi-phase fluid and multi-scale moving interfaces more accurately and intuitively.

(a) Prototype

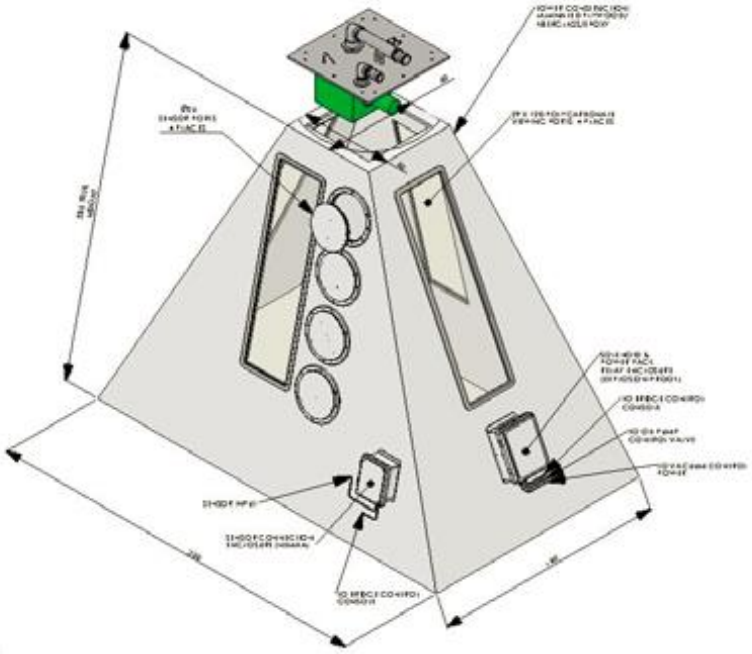

(b) Oil Skimming Tower with Vacuum Mechanism

Figure 1.1 The prototype catamaran equipped with oil skimming tower

1.5 Content of Thesis

Chapter 2, the experiments of the oil skimmer model conducted at Memorial University are described. The experiments were carried out to observe the oil recovery process. In Chapter 3, in order to verify the accuracy and capability of applying Star-CCM+ to solve various complicated hydrodynamic problems, a verification case is presented that involves three-phase flows, including oil, water and air. In Chapter 4, the computational domain for the hydrodynamic simulation of the oil skimmer using CFD method is described. The grid generation method is also given. The boundary conditions and initial conditions are presented. In Chapter5, the numerical results and analysis are described, along with the comparisons of experimental data and numerical results. The convergence studies for the hydrodynamic performance of the oil skimmer are also included. In Chapter 6, the optimization is presented. The optimization of skimming tower geometry, as well as the service speed of the oil skimmer, are investigated numerically. Future work and conclusions are given in Chapter 7. The numerical results of the current methods and models are concluded and reviewed. The recommendations are also given for further future work. Several future improvements for the optimization of the tower geometry are discussed in the future work section. The descriptions of the oil skimmer integrated into a catamaran are also included.

Chapter 2

Experiments

In this chapter, the experiment setup is presented. The apparatus of the tests, and the experiment conditions, including both of the initial condition and the final condition of the oil skimmer, as well as experimental results are described. The simplified oil skimmer applied in the validation experiments is also designed and introduced. The equations employed to calculate the numerical characteristics and the experimental properties are given.

2.1 Experimental Setup

Experiments for validating the hydrodynamic performance of the oil skimmer were conducted in the trim tank at Memorial University, NL, Canada. The dimension of the trim tank is 3.59m length, 1.2m width, and 0.995 m depth.

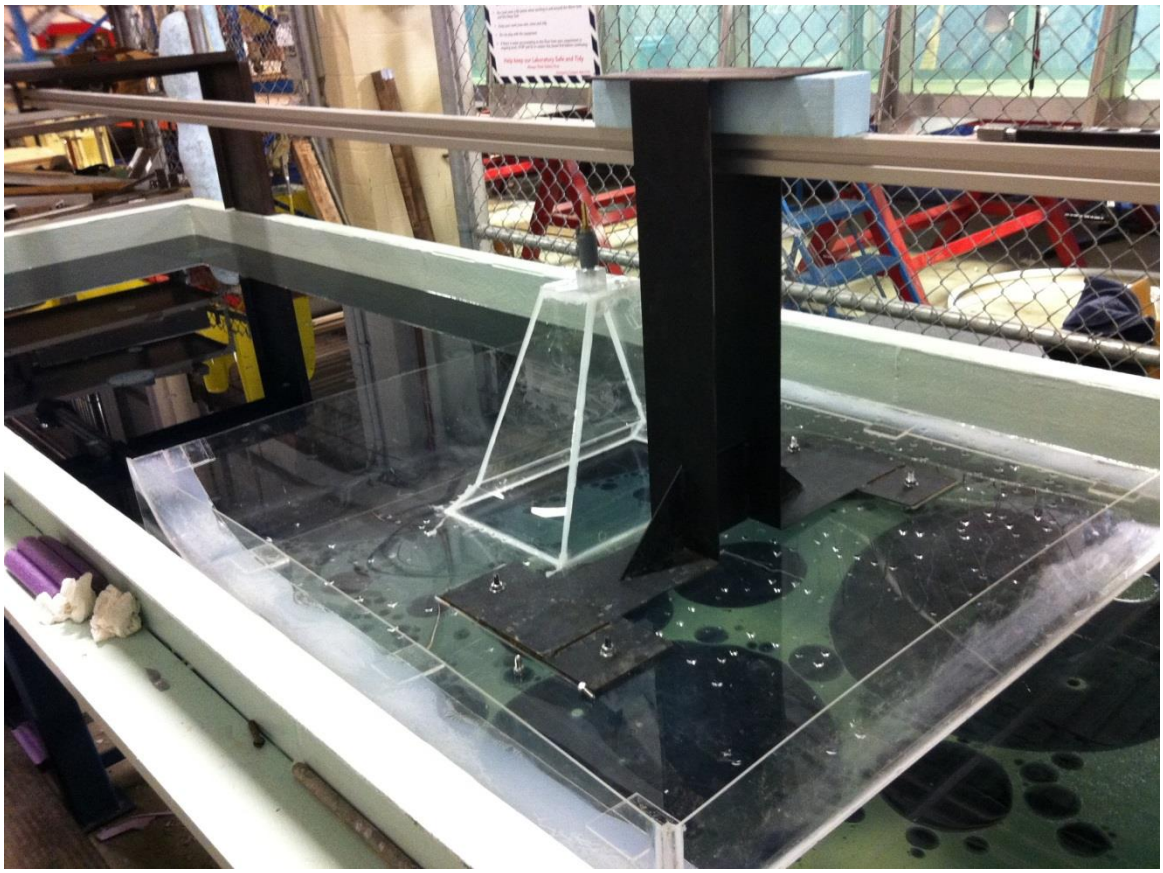

Figure 2.1 Trim tank at Memorial University and simplified skimmer model

The experiments were carried out to investigate the oil skimming process based on the vacuum mechanism. In the experiments, the interaction between the skimming tower and the vessel hull was assumed negligible. The main purpose of experiments was to observe the flow motion in the skimming tower. Hence, the simplified skimmer model, consisting of the skimming tower and the deck, was introduced, which did not consider the influence from the catamaran (Figure 2.1). The dimensions of the simplified oil skimmer are also outlined (Figure 2.2). The oil skimmer model used in the experiments was scaled down from the real prototype model. The base of the tower is $0.23m \times 0.35m$, and the height

of the tower is $0.30m$. It can be seen in the Figure 2.1 that the flat deck of the oil skimmer almost has the same width as that of the tank. This design was to lead the both sides of the model without free surface that could eliminate the effect from wave making. The design was also to reduce wall effect that the distance between the skimming tower and both sides is greater than that of the prototype oil skimmer.

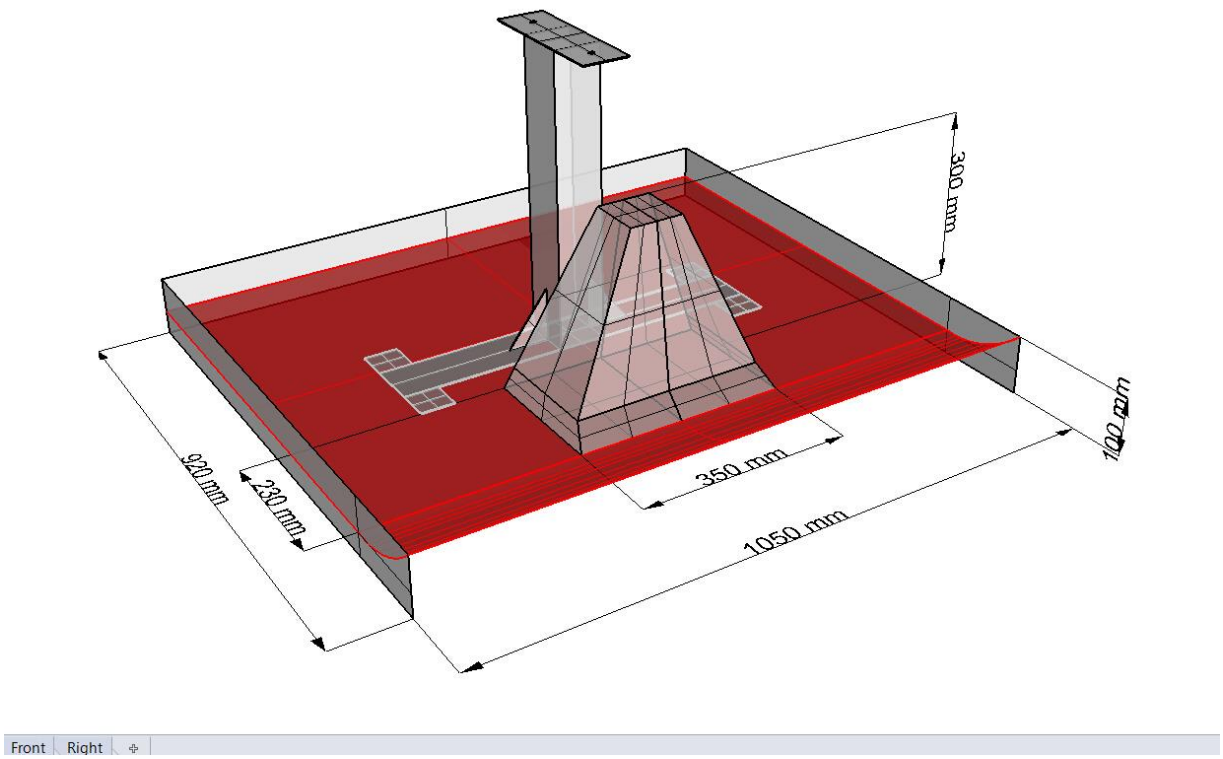

Figure 2.2 Prototype of the simplified oil skimmer with dimensions

The skimmer model was driven by a carriage with a 400W motor to keep the skimmer advancing at a constant speed. The experiments were conducted with different service

speeds. Since the speed of the prototype was given by EST, the service speed for the simplified oil skimmer in the lab corresponding to the Froude number can be determined. Thus, the numerical simulation was centered on the case with the constant speed, $u_0 = 0.527 m/s$.

The flat part of the deck was submerged about 32.0 mm under the water surface, where the value was measured in the lab, during operating the experiments. The trim angle was 0.7 degrees with stern down. Before advancing in the trim tank, the skimming tower was vacuumed by an air pump until the fluid mixture was at a certain height which was almost as the same height as the top of the tower. Then the air pump was turned off. The mixture of oil and water in the skimming tower was layered due to different densities. The air layer and oil layer in the tower before skimming were $d_{Air} = 28.0\ mm$ and $d_{Oil} = 20.0\ mm$, respectively. The water level in the tower was $d_{Water} = 240.0\ mm$ above the still water surface in the trim tank, which is corresponding to one atmospheric pressure. Note that the layers of air and oil inside the skimming tower are not necessary in the numerical simulation, while they existed in the experiments due to the principle of vacuum mechanism. The fresh water was also applied in the experiments. Since the air in the oil skimming tower cannot be pumped out completely to protect the safety usage of the air pump, the layer of air, d_{Air}, occurred that is allowed to be adjusted. In addition, when the air pump started working, the oil and water mixture would flow into the skimming tower so that the layer of oil, d_{Oil}, happened to stay above the layer of water because of the lighter density of oil.

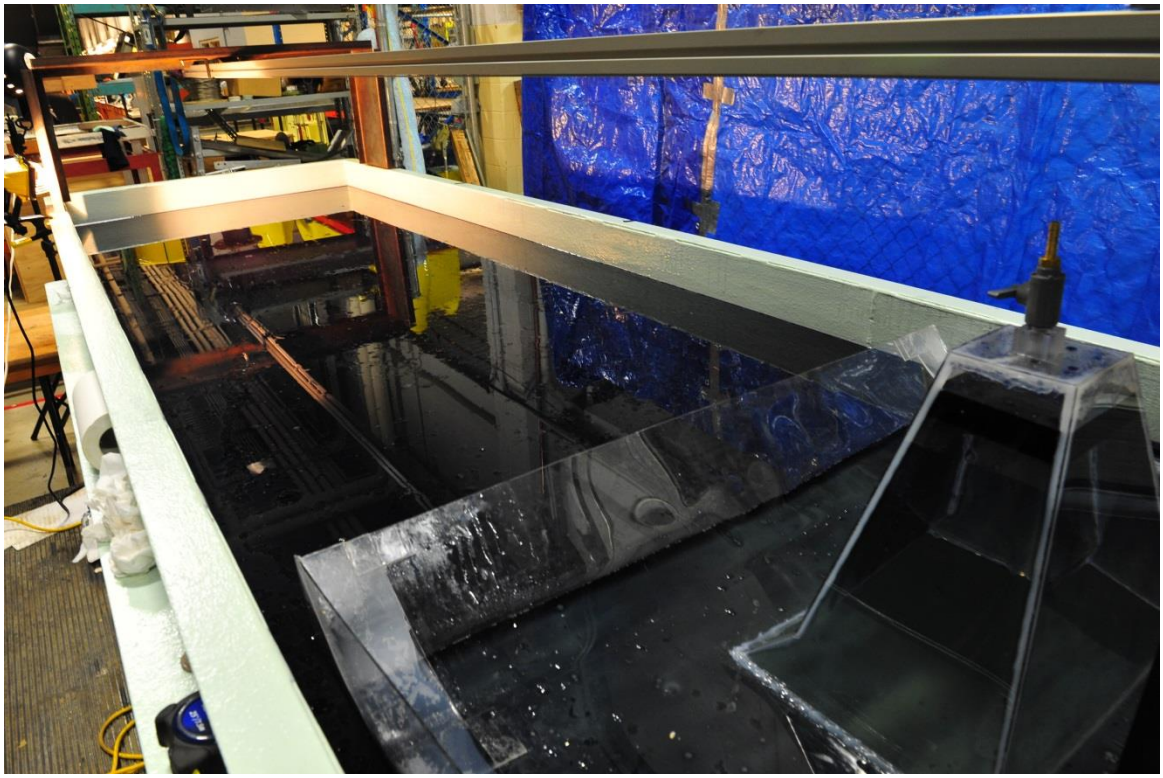

Figure 2.3 The initial condition of oil layer, water layer and air layer inside skimming tower (the level of black liquid represeted as oil while water level was beneth it)

Dyed vegetable oil was used in the tests, which is eco-friendly and easy to recover from the laboratory. According to the chemical tests of the dyed vegetable oil, the density is $\rho_{oil} = 920.0\ kg/m^3$ and the viscosity is $\mu = 0.0588\ Pa \cdot s$. The dyed vegetable oil was selected for the initial experiments, whereas other options of oil with similar chemical characteristics would be further investigated. The effects caused by different oil's characteristics would also be studied in the future work. The oil used in the experiments was dyed black and formed an oil film of a thickness of $\delta_{oil} = 2.0\ mm$ above the water

surface in the trim tank (Figure 2.3). A high speed camera was employed to capture the motions of fluid mixture in the skimming tower while it was advancing forward. The initial oil volume inside the skimming tower was measured. It took around 5 seconds for the oil skimmer travel from one end to the other end of the trim tank under the default speed. Figure 2.4 shows the final condition of the oil skimmer after 5 seconds. The final condition of the oil skimmer was captured. The final oil layer in the skimming tower was measured as $d'_{Oil} = 53.0\ mm$.

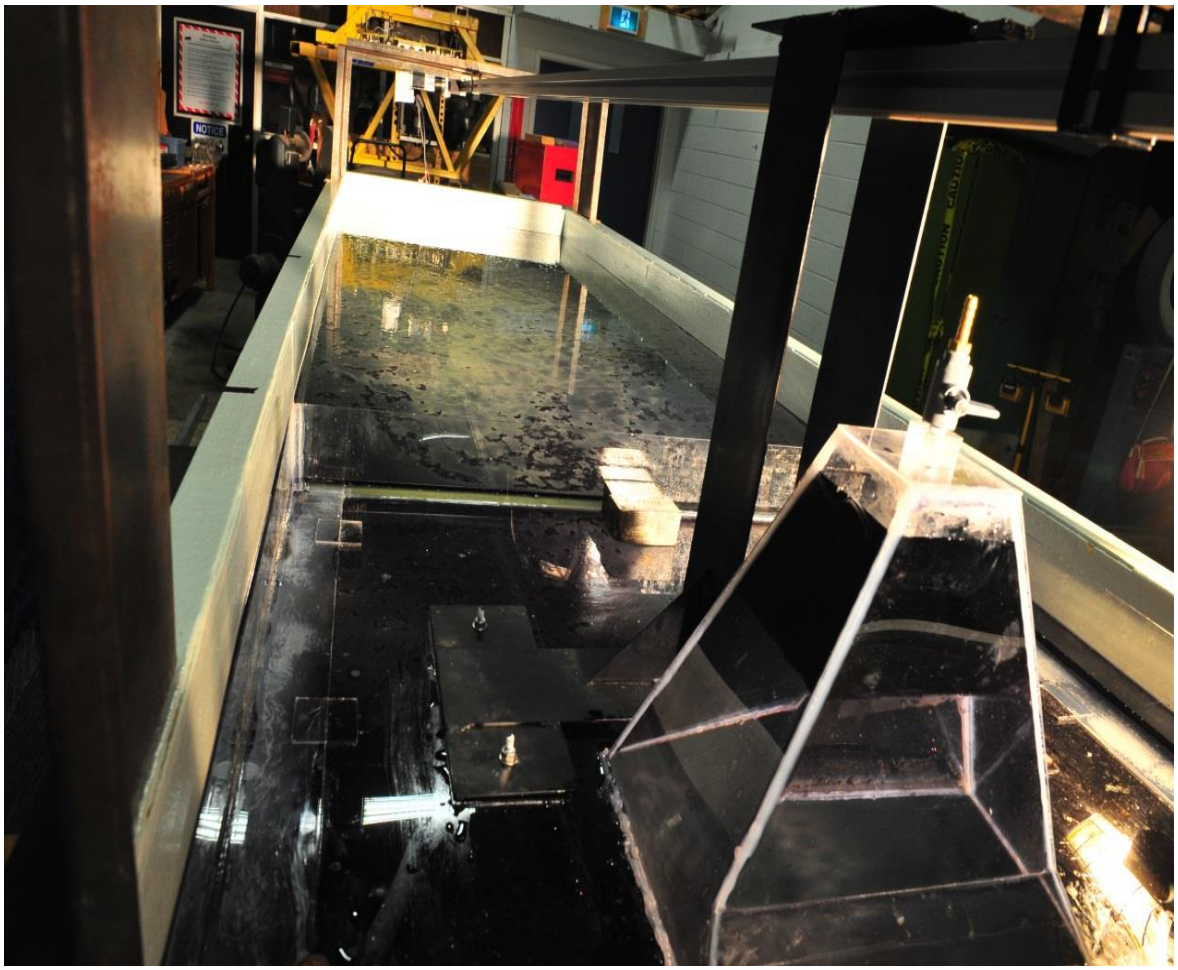

Figure 2.4 The final condition of oil skimmer model in the trim tank

2.2 Numerical Charateristics and Experimental Properties

The Froude number for the recovery vessel was calculated based on the definition of the Froude number of ship hydrodynamic performance. With respect to a ship, the Froude number is defined as:

$$Fn = \frac{v}{\sqrt{gL}} \tag{2.1}$$

where v is the velocity of the ship, g is the acceleration due to gravity and L is the length of the ship at the water line. The advancing speed of the oil skimmer was set to $u_0 = 0.527\ m/s$, which is corresponding to $Fn = 0.124$ of the recovery vessel.

All the experiment properties need to be obtained, i.e. the densities of oil, water and air, and the temperature in the experiment. The air inside the tower would be assumed as incompressible that means the density of air would remain the same value. The density of diluted air is calculated from the thermodynamic equation,

$$\rho_{Air} = \frac{p_{atm} - \rho_{Water} g d_{Water} - \rho_{Oil} g d_{Oil}}{RT} \tag{2.2}$$

where $g = 9.81\ m/s^2$, and the gas constant is $R = 287.058\ Nm/kg^{-1}K^{-1}$.

The absolute temperature is calculated by

$$T = 273.0 + t\ ℃\ (°K) \tag{2.3}$$

where the water temperature in the experiments was measured as $t = 20.0$ ℃ .

The water density was measured by MUN's Chemistry department, and is $\rho_{Water} = 997.56\ kg/m^3$. The oil density is $\rho_{Oil} = 920.0\ kg/m^3$ .Table 2.1 shows the fluid densities which were kept the same values in the numerical simulations.

Table 2.1 Densities of fluid in kg/m^3

Oil	Water	Air
920.0	997.56	1.17

Chapter 3

Verification Case Study

The verification case is about hydrodynamic simulation of a single gas bubble moving upwards in a rectangular tank which contains air, water and oil. It is a multi-phase fluid system that deals with liquid-liquid-gas problem. Prior to conduct the hydrodynamic simulation and optimization of the oil skimmer, this verification case was studied in order to verify that the commercial CFD software, Star-CCM+, is a reliable computation method for solving multi-phase flow problem.

3.1 Literature Review for the Verification Case

Kawano et al. (2007) have numerically and experimentally studied deformations of a gas bubble in liquid-liquid-gas systems. The boundary conditions of the gas bubble can be treated as no-slip wall, and the outer interface which is between oil and water for the spherical droplet can also be treated as no-slip wall. These boundary conditions ensure that the water would “encapsulate” the gas bubble when the gas bubble rises in the tank. Kawano et al. (2007) have also addressed deformation of a liquid shell in a uniform stream as a moving boundary problem of incompressible Navier-Stokes equations. Based on the experimental results from Kawano et al. (1996), the numerical solutions of deformation of liquid shells in liquid-liquid-gas systems were compared quantitatively.

In the paper of Kawano (1992), it clarified the drag coefficient of an encapsulated liquid drop moving with relatively high velocity. The drag coefficient of a spherical and concentric encapsulated liquid drop obtained up to Reynolds numbers of 200 for many kinds of physical properties by Kawano (1992). The empirical equations of drag coefficient suitable for a wide range of flow conditions were also introduced.

Kawano (1992) has made a few assumptions to introduce the governing equations based on the experimental results. In order to avoid the difficulties in experiments, the assumptions are applied in the theoretical analysis of the flow pattern around the encapsulated drop and the drag coefficient. These assumptions are also applied to the verification case. The fluids used here are Newtonian and the flow around the encapsulated drop is steady, viscous, incompressible and axisymmetric. The fluid physical properties are constant, including fluid temperature, and the effect of gravitational force is negligible. The effect of gas phase motion in the encapsulated drop is ignored because the gas viscosity and density are sufficiently small compared to those of the liquid. The encapsulated drop consists of a spherical gas bubble coated with a concentric liquid film. The oscillation and the rotation of the encapsulated drop interfaces are neglected.

The Navier-Stokes equations as the governing equations introduced by Kawano (1992) employed by the verification case in terms of the stream function $\emptyset_i$ and the vorticity ω_i are written in spherical coordinates below.

$$E^2 \emptyset_i = \omega_i r \cdot \sin\theta$$

$$\frac{\hat{R}e_i}{2}\left\{\frac{\partial \emptyset_i}{\partial r}\cdot\frac{\partial}{\partial\theta}\left(\frac{\omega_i}{r\cdot\sin\theta}\right)-\frac{\partial \emptyset_i}{\partial\theta}\cdot\frac{\partial}{\partial r}\left(\frac{\omega_i}{r\cdot\sin\theta}\right)\right\}\sin\theta = E^2(\omega_i r\cdot\sin\theta)$$

where

$$E^2 = \frac{\partial^2}{\partial r^2}+\frac{\sin\theta}{r^2}\cdot\frac{\partial}{\partial\theta}\left(\frac{1}{\sin\theta}\cdot\frac{\partial}{\partial\theta}\right)$$

Subscript i is equal to 1 or 2 and indicates liquid 1 or liquid 2, respectively.

The continuity equations are satisfied when the velocity components u_i are related to $\emptyset_i$ in the following equations.

$$u_{r,i} = \frac{-1}{r^2\cdot\sin\theta}\cdot\frac{\partial \emptyset_i}{\partial\theta}$$

$$u_{\theta,i} = \frac{1}{r\cdot\sin\theta}\cdot\frac{\partial \emptyset_i}{\partial r}$$

where r and θ indicate the radial direction and the tangential direction, respectively.

Kawano (1992) developed a numerical analysis method to solve the governing equations at finite Reynolds number. An exponential step size in the radial direction is used, and the governing equations can be written as the finite difference equations using the centered spatial differences of second-order accuracy. These transformed equations are solved by the successive over relaxation method.

3.2 Numerical Results from Star-CCM+

In the verification case, the drag coefficient for the encapsulated drop and the deformation ratio of the gas bubble are investigated numerically by exporting data from Star-CCM+.

The diameters and the velocity of the encapsulated drop are exported by a constant time interval. Since the values of velocity can be obtained from Star-CCM+, the corresponding Reynolds number can be calculated in the following equation.

$$Re = \frac{d_0 U}{v}$$

where d_0 is the equivalent diameter of the encapsulated drop, U is the velocity of the encapsulated drop and v is kinematic viscosity.

The deformation ratio of the encapsulated drop is determined by the deformable diameter of the encapsulated drop introduced by Kawano (2007). The deformation ratio, ϑ, can be expressed in the following.

$$\vartheta = \frac{d_r}{d_z}$$

where d_r is the horizontal diameter of the encapsulated drop and d_z is the vertical diameter of the encapsulated drop.

Thus, the equivalent diameter of the encapsulated drop is evaluated in the following equation.

$$d_0^3 = d_z d_r^2$$

The relationship between *Re* and the deformation ratio ϑ is shown below. It can be found that ϑ increases as *Re* increases, which agrees well with Kawano (1992).

The screen shots from Star-CCM+ of the gas bubble rising in the tank are compared with those taken by the high speed camera by Kawano (2007). The numerical simulation in Star-CCM+ has the same conditions with those in Kawano (2007). They have reasonable agreements with the experimental results. The slight differences occurred are most probably due to the size and quality of mesh applied in the Star-CCM+.

From the screen shots shown below, it is found that t^d is the time of the encapsulated drop starting to move through the interface of two liquids. The color contours are also presented in the following screen shots. The volume fractions of oil, ink-water and gas-bubble are represented by different colors. The scales of these volume fractions are from 0.5 to 1.0.

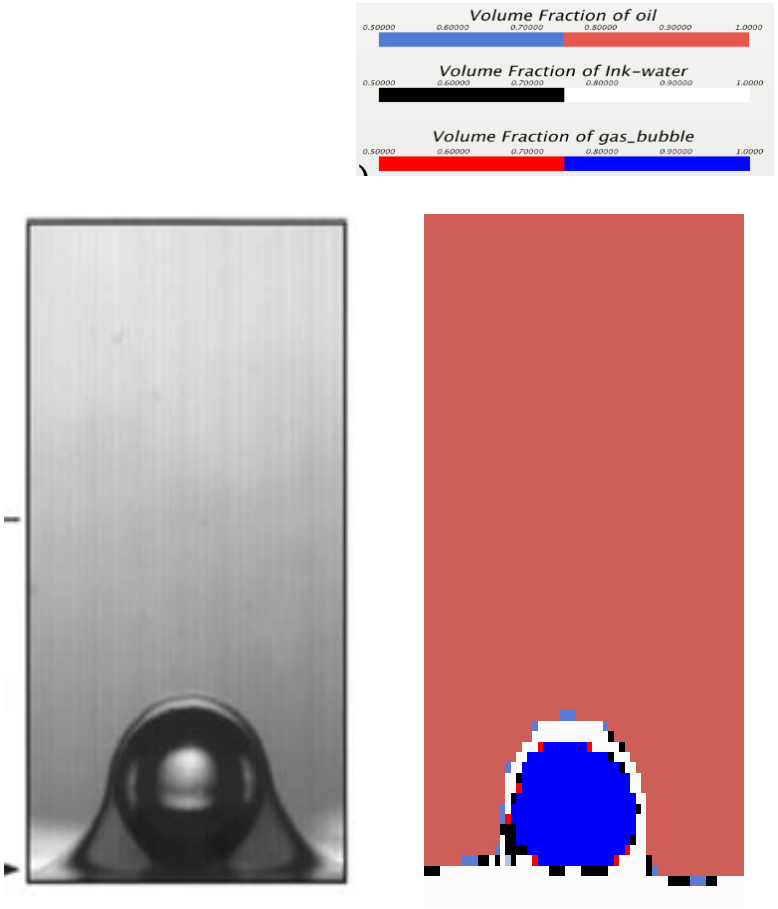
Volume Fraction of oil
0.50000 0.60000 0.70000 0.80000 0.90000 1.0000
Volume Fraction of Ink-water
0.50000 0.60000 0.70000 0.80000 0.90000 1.0000
Volume Fraction of gas_bubble
0.50000 0.60000 0.70000 0.80000 0.90000 1.0000

$t^d = 0.0\ sec$

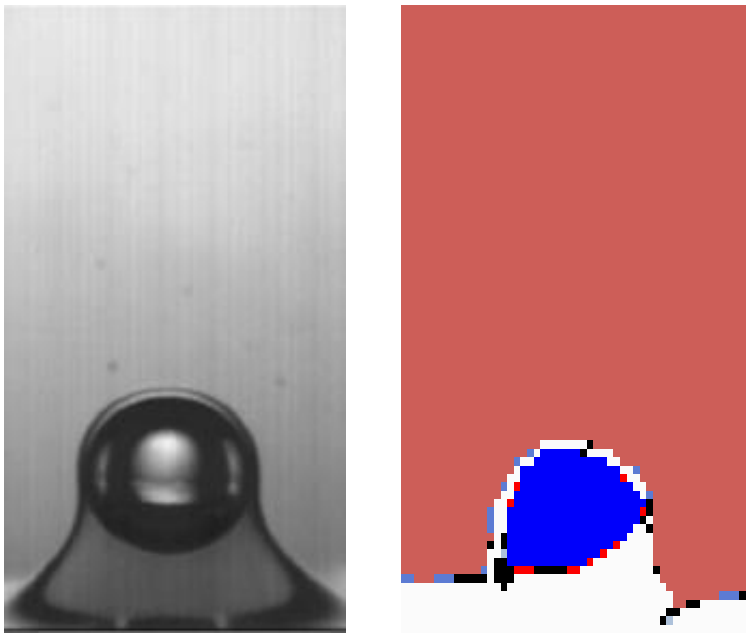

$t^d = 0.01\ sec$

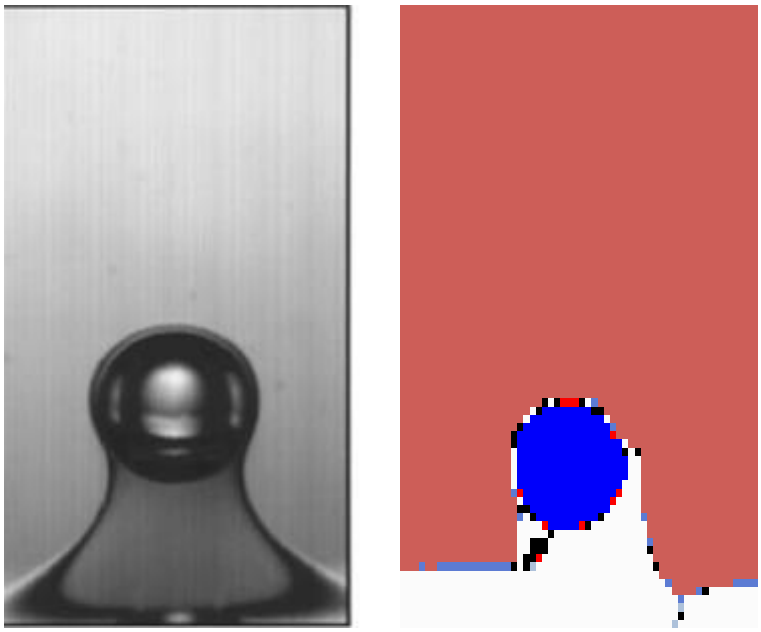

$t^d = 0.02\ sec$

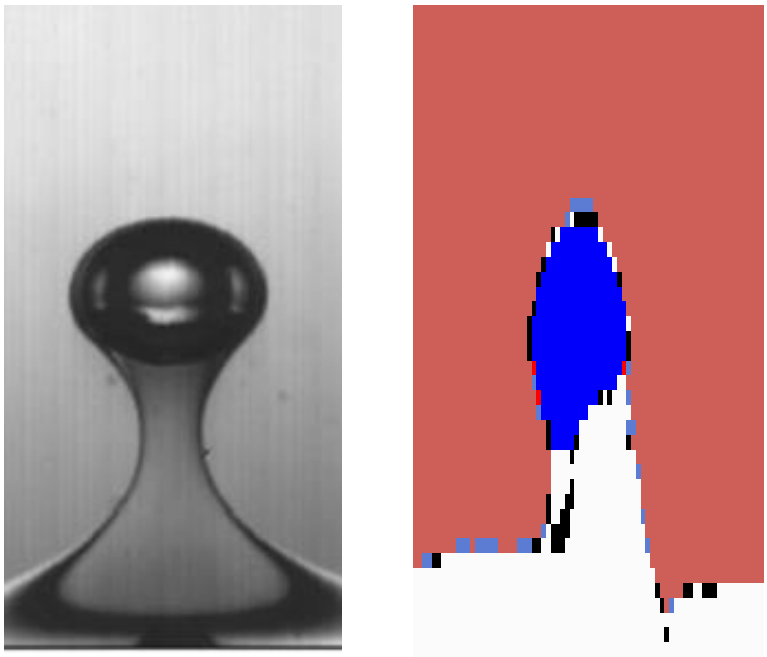

$t^d = 0.03\ sec$

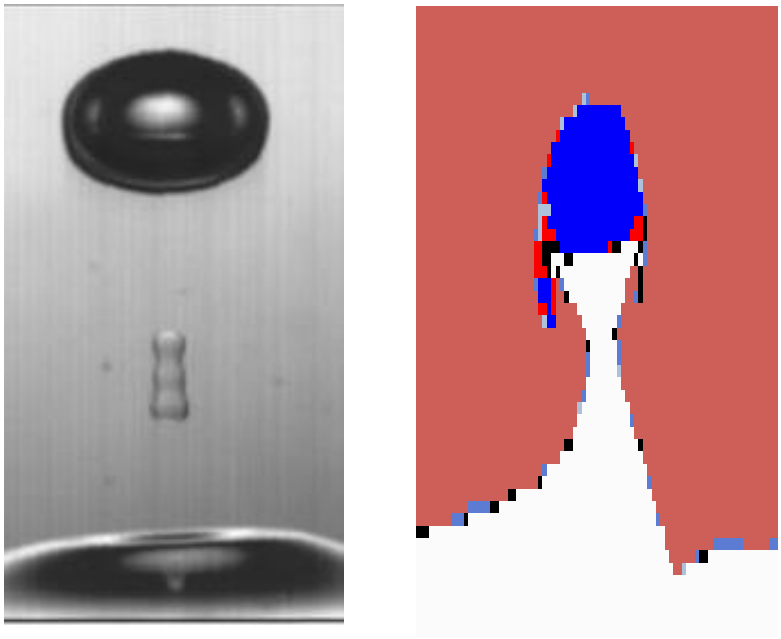

$t^d = 0.04\ sec$

Fig 3.1 Comparison of the screen shots of numerical results and experimental results

Since the drag coefficients of the encapsulated drop cannot be obtained directly from Star-CCM+, an empirical equation of drag coefficient, C_d, is introduced. Kawano (1992) has proved this empirical equation of C_d is reliable for various Re and is able to solve most of numerical analytical problems. Kawano (1992) developed the empirical equation of drag coefficients for the encapsulated drop in the following.

$$C_d = \frac{0.195}{2.25^n} \cdot A^{2n+1}\{1 + \frac{9.06}{\sqrt{Re}}(\frac{1.5}{A})^n\}^2$$

where A is dimensionless parameter corresponding to1 for the gas bubble and 1∼1.5 for the liquid drop or for the encapsulated drop; n is the selected coefficient equaling to 1.9 for most cases.

This equation is also available for estimating C_d in the verification case. The values of Re are obtained from the exported data in Star-CCM+. The relationships of C_d, Re and deformation ratio ϑ are discussed in the following section. The comparison results of the verification case and Kawano (1992) are also investigated.

The numerical results calculated from the program are presented in the following table. They are computed based on the exported data in Star-CCM+. The variables required in the empirical equations are mostly obtained.

Table 3.1 Numerical results calculated for the verification case

real time	0.01 sec	0.06 sec	0.12 sec	0.18 sec	0.24 sec
equivalent diameter (m)	5.10363E-03	5.47734E-03	5.57791E-03	5.61727E-03	6.81642E-03
deformation ratio	1.03125E+00	1.01136E+00	1.13953E+00	1.83333E+00	2.09756E+00
dimensionless coefficient A	1.47433E+00	1.47433E+00	1.46598E+00	1.46284E+00	1.39257E+00
d_equivalent/d_gasbubble	1.05333E+00	1.05333E+00	1.07267E+00	1.08024E+00	1.31085E+00
Re	350.00	620.00	780.00	890.00	970.00
Velocity (m/s)	8.37E-02	1.38E-01	1.71E-01	3.30E-01	2.96E-01
Drag coefficient Cd	6.06136E-01	5.09768E-01	4.69643E-01	4.50821E-01	3.64906E-01

3.3 Comparison Results

The numerical results of the verification case from Star-CCM+ are compared with the analytical and numerical solutions from Kawano (1992). The relationships of deformation ratio of the encapsulated drop and *Re* are plotted in the following.

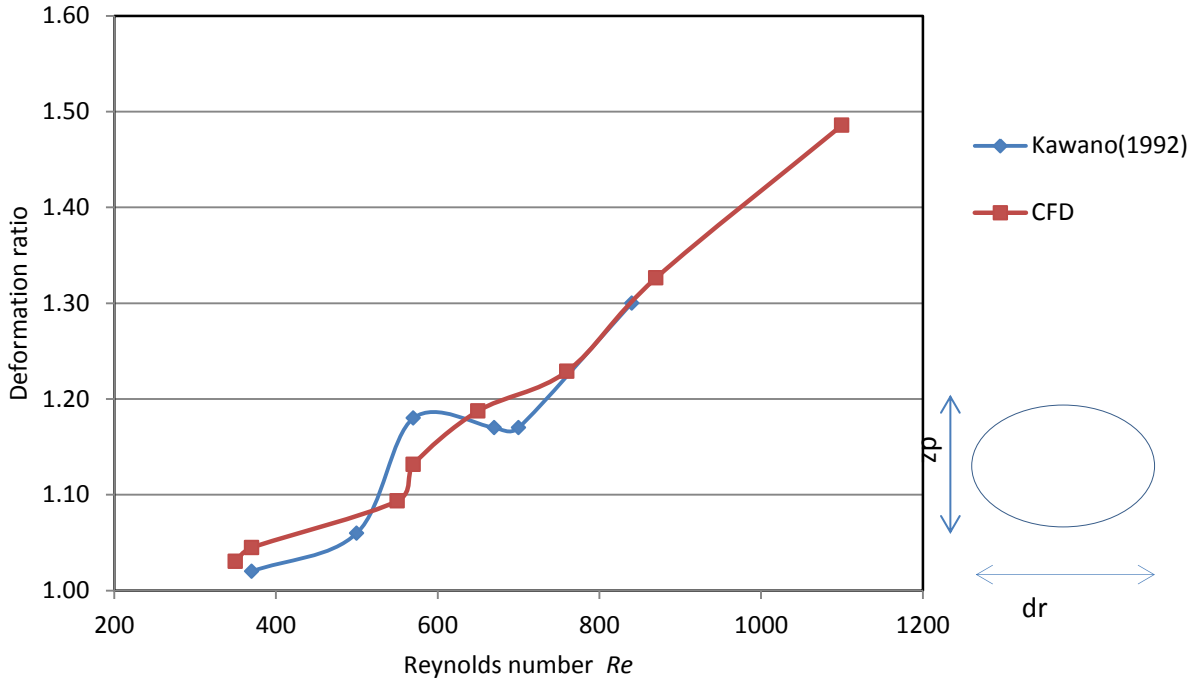

Figure 3.2 Comparison results of relationships of deformation ratio to *Re*

From Figure 3.2, it is found that the results from Star-CCM+ have the same tendency with those of Kawano (1992). The deformation ratio of the encapsulated drop increases as *Re* increases. When the Reynolds number is greater than 300 and smaller than 800, the values of deformation ratio from Star-CCM+ are less than those from Kawano (1992).

The compared relationships of drag coefficient to Reynolds number are presented in the following. At $Re = 0.1$, the value of C_d in Kawano (1992) is equal to 233 and the numerical value from Star-CCM+ is equal to 240. The deviation rate between them is 3%, where the values of the deviation rate would decrease as Re increases (Figure 3.3). When $Re = 8$, the two curves have an interception point which means the drag coefficients of

both cases are the same. The deviation rate would increase while the Reynolds number are increasing after the interception point.

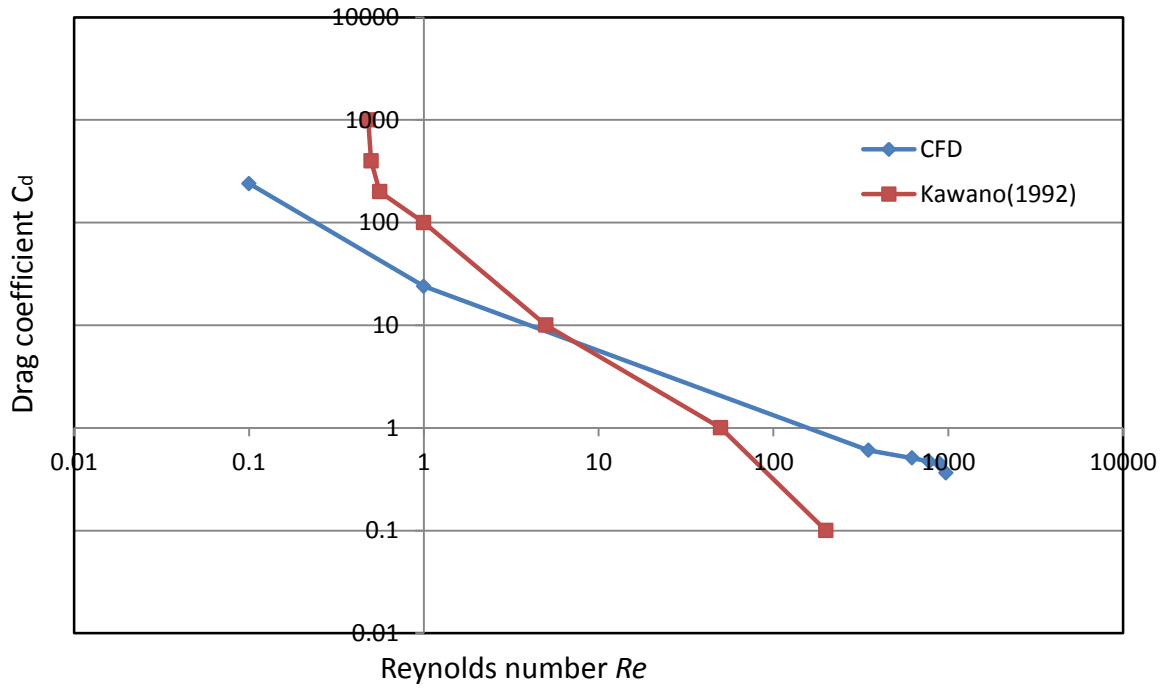

Figure 3.3 Comparison results of relationships of drag coefficient to *Re*

The numerical results from Kawano (1992) and Star-CCM are compared analytically. It still has a few improvements for the verification case. The finer mesh can be applied within this simulation case. The number of grids used in Star-CCM+ was about 2.3 million. The time step applied here was 0.001 sec while it can be varied in order to obtain a better outcome. However, the solutions from this verification case agree reasonably with the existing numerical results in Kawano (1992) based on the same time interval screenshots. Figure 3.2 and 3.3 have also presented the results obtained from CFD

method and the studies of Kawano which are numerically matchable. It can be found that the commercial CFD software, Star-CCM+, is reliable for solving multi-phase and multi-scale flow problems.

Chapter 4

Numerical Simulation

In the numerical simulation, the recovery process was simplified into a three-phase flow problem involving oil, water and air. It was simulated by using commercial CFD software, Star-CCM+. The Volume of Fluid (VOF) method is employed to analyse the moving surfaces between the fluid phases. This chapter provides the whole process of the numerical simulation applied in the CFD software. It also gives the mathematical model, computational domain in CFD, and grid generation method for simulating the hydrodynamic performance of the oil skimmer.

4.1 Mathematical Model

The Reynolds Averaged Navier-Stokes (RANS) equations are solved for the three-phase turbulent flow including oil, water and air. Since the velocity of the oil skimmer is small, the fluid in the skimming tower can be seen as incompressible flow, where RANS can be applied to solve incompressible flow. In this case, the density of air inside the tower can be treated as constant value, i.e. $\rho_{air} = 1.17\ kg/m^3$. The coordinate system is defined with a positive *z*-axis upwards and a positive *x* in the upstream direction, where the coordinates (*x*, *y*, *z*) are represented by $x_j (j = 1, 2, 3)$, respectively.

$$\frac{\partial u_j}{\partial x_j} = 0 \tag{4.1}$$

$$\rho \frac{\partial u_i}{\partial t} + \rho \frac{\partial u_i u_j}{\partial x_j} = -\frac{\partial p}{\partial x_i} + \frac{\partial}{\partial x_j}\left[\mu\left(\frac{\partial u_i}{\partial x_j} + \frac{\partial u_j}{\partial x_i} - \frac{2}{3}\delta_{ij}\frac{\partial u_l}{\partial x_l}\right)\right] + \frac{\partial}{\partial x_j}\left(-\rho\overline{u_i' u_j'}\right) + f_i \ (i = 1, 2, 3) \tag{4.2}$$

where Einstein summation notation is used.

The average velocity components along *x*-, *y*- and *z*- axes are denoted by u_i, and u_i is equal to $U_i - u_i'$ where U_i is the instantaneous velocity and u_i' is the turbulent velocity. The variables showed in Equation (2) are presented that ρ is the density of water, oil or air; p is the pressure; μ is the dynamic viscosity of water, oil or air. f_i represents the external force which is gravity force in this case. The continuity equation (Equation (1)) and the transportation equations of momentum (Equation (2)) govern the pressure p and the velocity components u_i. δ_{ij} in Equation (2) is the Kronecker delta, and its function is shown below.

$$\delta_{ij} = \begin{cases} 0, & if\ i \neq j \\ 1, & if\ i = j \end{cases} \tag{4.3}$$

$-\rho\overline{u_i' u_j'}$ is always known as the turbulence term or the Reynolds stress. The SST $k - \omega$ eddy viscosity model developed by Menter (1994) was employed in this numerical simulation. $-\rho\overline{u_i' u_j'}$ can be solved in two means, one is using the eddy viscosity model based on the Boussinesq hypothesis, while the other is applying the transport equation

based on Reynolds stress model. The Reynolds stresses are computed in the following equation that the eddy viscosity μ_t can be obtained accoriding to the Boussinesq hypothesis.

$$-\rho\overline{u_i'u_j'} = \mu_t\left(\frac{\partial u_i}{\partial x_j}+\frac{\partial u_j}{\partial x_i}\right) - \frac{2}{3}\left(\rho k + \mu_t\frac{\partial u_i}{\partial x_i}\right)\delta_{ij} \tag{4.4}$$

In Equation (4), the eddy viscosity, $\mu_t = \rho k/\omega$, where k is the turbulence kinetic energy and ω is the specific turbulence kinetic energy dissipation rate. In order to obtain k and ω, the transportation equations can be applied below.

$k - equation$:

$$\frac{\partial(\rho k)}{\partial t}+\frac{\partial}{\partial x_j}\left(\rho U_j k\right) = \frac{\partial}{\partial x_j}\left[\left(\mu+\frac{\mu_t}{\sigma_k}\right)\frac{\partial k}{\partial x_j}\right] + P_k - \beta`\rho k\omega + P_{kb} \tag{4.5}$$

$\omega - equation$:

$$\frac{\partial(\rho\omega)}{\partial t}+\frac{\partial}{\partial x_j}\left(\rho U_j \omega\right) = \frac{\partial}{\partial x_j}\left[\left(\mu+\frac{\mu_t}{\sigma_\omega}\right)\frac{\partial \omega}{\partial x_j}\right] + a\frac{\omega}{k}P_k - \beta`\rho\omega^2 + P_{\omega b} \tag{4.6}$$

where P_k is the production rate of turbulence, which is calculated in the following equation

$$P_k = \mu_t\left(\frac{\partial U_i}{\partial x_j}+\frac{\partial U_j}{\partial x_i}\right)\frac{\partial U_i}{\partial x_j} - \frac{2}{3}\frac{\partial U_k}{\partial x_k}\left(3\mu_t\frac{\partial U_k}{\partial x_k}+\rho k\right) \tag{4.7}$$

$$P_{kb} = -\frac{\mu_t}{\rho\sigma_\rho}g_i\frac{\partial \rho}{\partial x_i} \tag{4.8}$$

$$p_{\omega b} = \frac{\omega}{k}\left((\alpha+1)C_3 max(P_{kb},0) - P_{kb}\right) \tag{4.9}$$

where C_3 is dissipation coefficient, $C_3 = 1$.

The constants from this turbulence model are given by:

$$\beta` = 0.09$$

$$\alpha = \frac{5}{9}$$

$$\beta = 0.075$$

$$\sigma_k = 2$$

$$\sigma_\omega = 2$$

The two additional transportation equations, Equations (5) and (6) for k and ω are solved independently in an inner iteration, then they are coupled with the governing equations (Eqn. (1), (2)) after the inner iteration is completed.

4.2 Numerical Model for Oil Skimmer

Since the verification case of the three-phase flow problem has been successfully analysed by Star-CCM+, the numerical model for oil skimmer can be simplified to deal with a three-phase flow problem. In the experiment, the density of air inside the skimming tower is different with the atmospheric air density that leads to a four-phase flow condition (Figure 4.1 (A)). However, in order to reduce the difficult levels of computation with the already known computing accuracy of Star-CCM+ in three-phase flow problem, the numerical model can be simplified into an internal flow model which has three-phase condition. The simplified numerical model (Figure 4.1 (B)) has a flat deck that is extended from the arc deck existing in the simplified experimental model. This flat deck is right on the water line that can separate the atmospheric air and the internal flow, which leads to a three-phase flow condition.

When the numerical model is under three-phase flow condition, the free surface occurred in front of the oil skimmer model can be neglected. The effect of wave making to the oil and water mixture flowing into the oil skimming tower can also be ignored.

The difference between the oil skimmer model used for experiments and the numerical model can be seen in Figures 4.1 (A) and (B).

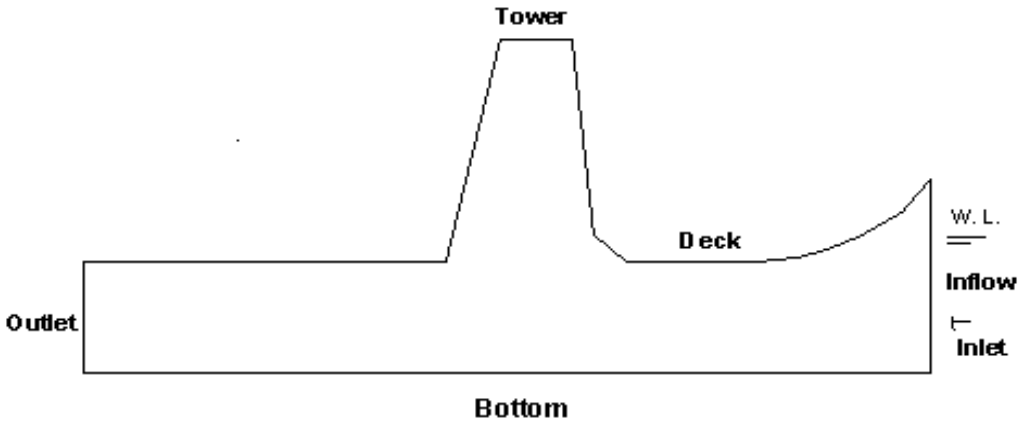

(A) The simplified oil skimmer model for experiments

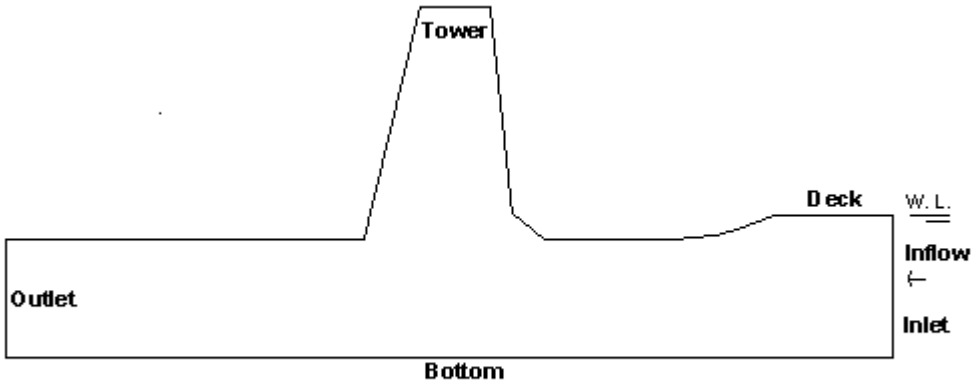

(B) The simplified oil skimmer model for numerical simulation

Figure 4.1 Comparison of oil skimmer model for experiments and numerical simulation

4.3 Computational Domain

The three dimensional computational domain is presented below (Figure 4.2), and the two dimensional top view and side view are also showed in the following (Figures 4.3 and 4.4). Since the scale used in the numerical simulation was kept the same as those in the experiments, the numerical results can be directly compared to the experimental data without involving scaling. This can help the numerical results look more straight forward during the data analysis. The computational domain is $1.108 \times 1.05 \times 0.15$ m. The front end of the sloping deck is about 32.0 mm higher than the base of the trim tank in which the coordinate $z - axis$ was set as zero. This height is denoted h_0.

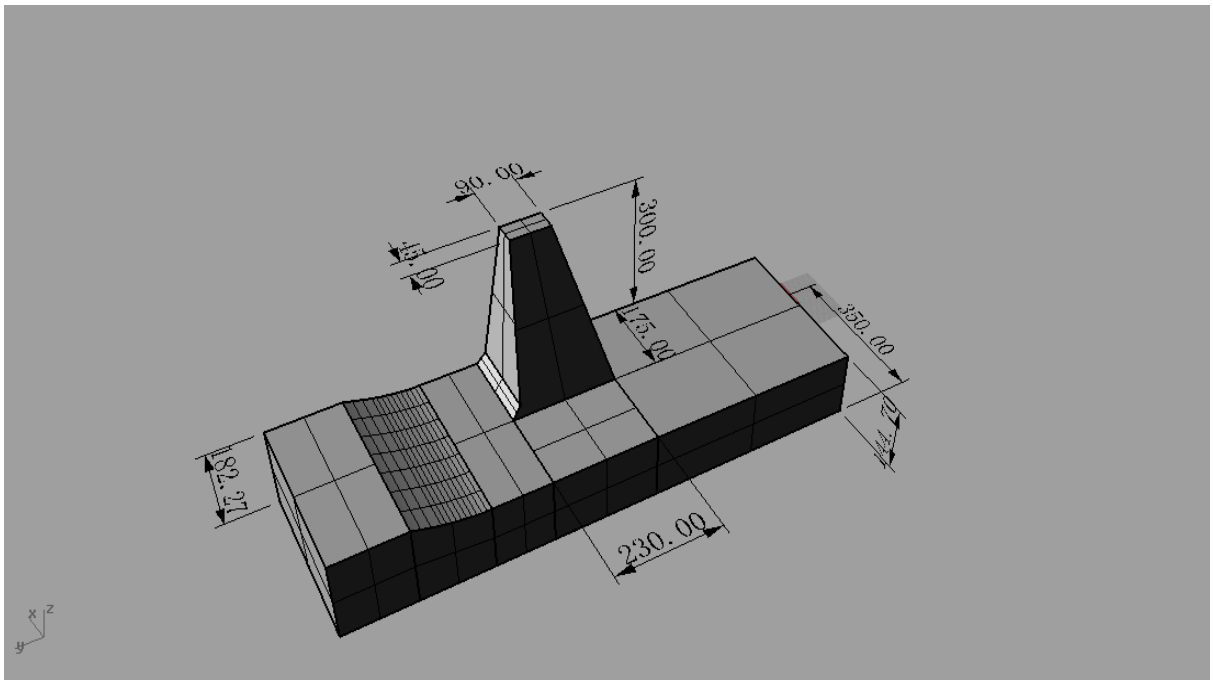

Figure 4.2 Three dimensional computational domain with dimensions (units, mm)

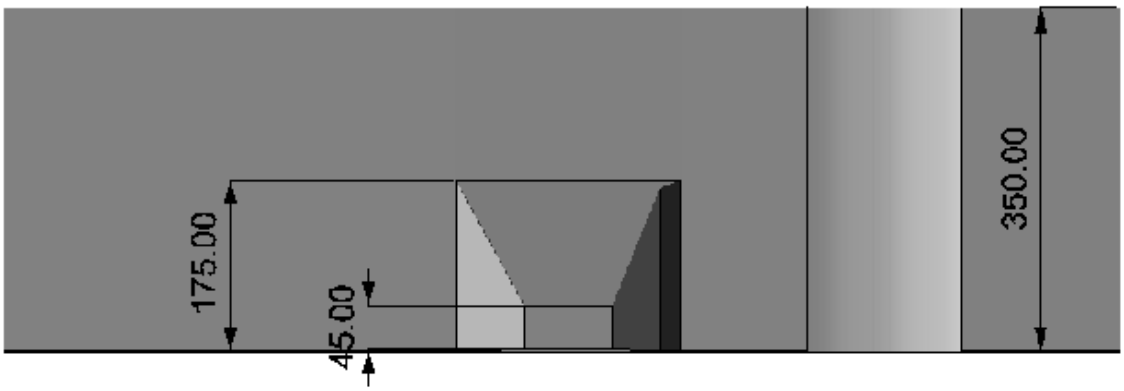

Figure 4.3 Two dimensional top view of computational domain with dimensions (units, mm)

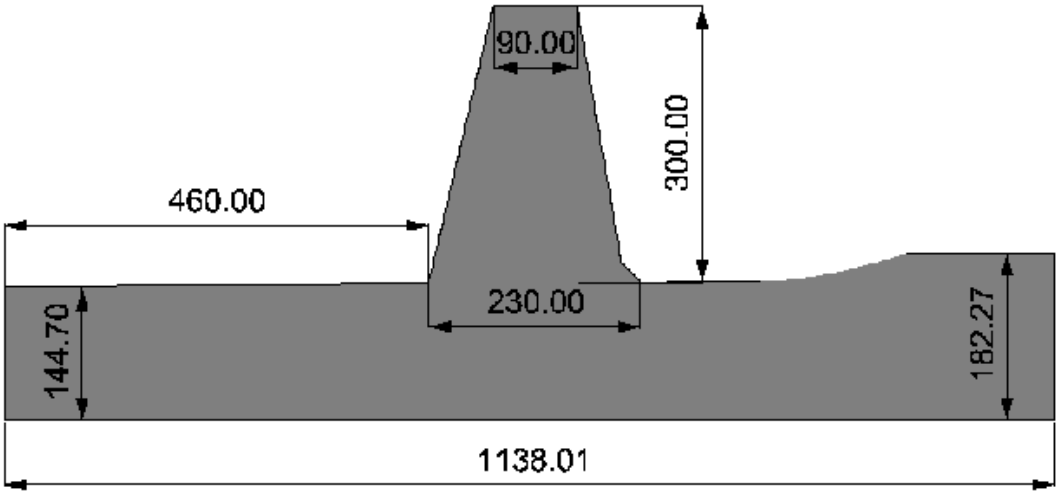

Figure 4.4 Two dimensional side view of computational domain with dimensions (units, mm)

The effect of free surface in front of the sloping deck can be neglected due to the low advancing speed which is with the Froude's number $Fn = 0.124$. In this case, the flow underneath the slopping deck is treated as a channel flow without free surface. It can be also assumed that oil, water and diluted air in the tower are incompressible during the oil recovery process.

Since the gap between the side wall of trim tank and the side edge of the oil skimmer model was always kept sufficiently small in the experiments, the effect of free surface on the side wall can be ignored. In addition, this computational domain can be considered as a symmetric model based on the flow conditions. This simulation was centred on the half geometry which required less mesh number and could be more time cost effective.

4.4 Initial Conditions and Boundary Conditions

The top of the slopping deck in the front is corresponding to 1 atmospheric pressure that is defined as p_0. The static pressure, denoted as h_{sta}, of an arbitrary point inside the skimming tower is calculated by the equations below.

$$p_{sta} = \begin{cases} p_0 + \rho_{Air} g(h - h_{Oil}) + \rho_{Oil} g d_{Oil} + \rho_{Water} g(h_{Water} - h_0) & if\ h_0 > h_{Oil} \\ p_0 + \rho_{Oil} g(h - h_{Water}) + \rho_{Water} g(h_{Water} - h_0) & if\ h_{Oil} > h > h_{Water} \\ p_0 + \rho_{Water} g(h - h_0) & if\ h < h_{Water} \end{cases} \quad (4.10)$$

where h is the height that is the z component of an arbitrary point in the skimming tower, $h_{Oil} = 240.0$ mm is the height of the upper level of oil layer and $h_{Water} = 220.0$ mm is the height of the upper level of water layer. These values were maintained as same as those in the experiments. The origin of this coordinate system is set at the base of the skimming tower.

The slip wall boundary condition was applied on the tower surface and the deck surface. The symmetric boundary condition was applied on the central plane. The inflow velocity was imposed on the side, bottom, inlet and outlet boundaries under the deck.

The initial thickness of air layer on the top of the tower after turning off the air pump is $d_{Air} = 28$ mm, and the thickness of oil layer in the tower, $d_{Oil} = 20$ mm, is below the air

layer. The thickness of oil slick formed right underneath the deck surface is $\delta_{Oil} = 2.0$ mm. As observed in the experiments, the oil slick was spread on the top surface of the trim tank except the base of the skimming tower after the air pump was off. The volume of oil used in the experiments was 7.93 L. In order to maintain the same physical conditions with the experiments, the volume fraction of oil in the base of the skimming tower can be set as 0.0, while the volume fraction of water there can be set as 1.0 during the CFD simulation.

The volume fractions defined in the computational domain are based on the theory of the total value of volume fractions for a three-phase flow, where the total value is equal to 1.0. Hence, the volume fractions, $F_{Oil} = 1.0$, $F_{Air} = 0.0$, and $F_{Water} = 0.0$, were set in the both oil layers in the computational domain, in which they can be applied by User Define Function (UDF). Similarly, $F_{Oil} = 0.0$, $F_{Air} = 1.0$, and $F_{Water} = 0.0$, were for the grids in the air regions, along with $F_{Oil} = 0.0$, $F_{Air} = 0.0$, and $F_{Water} = 1.0$ were set in the water regions. The relationship of the total volume fractions, $F_{Oil} + F_{Air} + F_{Water} = 1.0$, that needs to be satisfied at any time in all the grids, should be always considered.

Based on the practical condition in the experiments, the oil skimmer had a linear acceleration to achieve the constant speed, $u_0 = 0.527 m/s$, when it was advancing in the trim tank. In the numerical simulation, the velocity of the oil skimmer, u_t, can be expressed as

$$u_t = \begin{cases} u_0 & t \geq t_0 \\ \frac{u_0 t}{t_0} & t < t_0 \end{cases} \tag{4.11}$$

where the accelerating time t_0 is given as $1.0s$. The velocity of the inflow can be defined as above, where the physical condition is setup. Table 4.1 (A) and (B) shows the other initial conditions and boundary conditions related to the numerical simulations, respectively, which are obtained from Star-CCM+.

Table 3.1 (A) Intial conditions in the numerical simulations

Atmospheric pressure	101325.0 pa
Pressure	Static
Velocity	0.0 m/s
Specific dissipation rate	1.0 E-4/s
Turbulent kinetic energy	0.0010 J/kg
Fraction in oil region	$F_{oil} = 1$, F_{water}=0, F_{air}=0
Fraction in water region	$F_{oil} = 0$, F_{water}=1, F_{air}=0
Fraction in air region	$F_{oil} = 0$, F_{water}=0, F_{air}=1

Table 3.1 (B) Boundary conditions in the numerical simulations

Skimming tower	Wall
Deck	Wall
Central plane	Symmetric plane
Inflow	Velocity inlet
Side	Velocity inlet
Bottom	Velocity inlet

4.5 Grid Generation

The computational domain is discretized into structural grids. In order to resolve the transition of density and viscosity for the three-phase flow, the grids close to the phase

interface must be particularly fine. The first spacing was chosen as $y^+ \leq 10$. y^+ could be calculated in the following equations based on the instructions from Star-CCM+ manual. Sufficient grids should be distributed within the thin oil layer and in the tower to capture the motions of oil drops. Table 4.2 also presents the information of grids size used in the numerical simulation. The equations below can be referred to the Star-CCM+ manual.

$$y^+ = \frac{u^* y}{v} \tag{4.12}$$

where $u^* \approx \sqrt{\frac{\tau_w}{\rho}}$, the wall shear stress τ_w can be related to the skin friction coefficient

$$\overline{C_f} = \frac{\tau_w}{\frac{\rho U^2}{2}} \tag{4.13}$$

The skin friction coefficient can be estimated from correlations

$$\frac{\overline{C_f}}{2} = \frac{0.036}{Re^{\frac{1}{5}}} \tag{4.14}$$

where Re is the Reynolds number.

Table 4.2 Grid size used in the numerical simulation

Number of prism layers	5
Prism layer thickness	6.0 E-4 m
Minimum volume mesh size	6.6 E-4 m
Maximum volume mesh size	0.12 m
Ratio=maximum grid size/minimun grid size	181.81
y^+ (with the velocity of 0.512 m/s)	2.3

The CFD simulation was specially focused on one set of mesh that the number of grids is 16.2 million grids. There are four sets of mesh been completed for the convergence studies. The numerical results showed that the mesh with 16.2 million grids was a more appropriate selection which has the most time cost effective. In the grid generation, a variable, n_δ, was introduced to define the ratio of the thickness of the oil layer, δ_{Oil}, to the vertical dimension of the grid. A variety of grid number was employed to control the grid resolution in the oil layer. The grids distribution in the computational domain with various n_δ in different blocks is also presented in Figure 4.5. It can be seen that $n_\delta = 3.0$ in Block A and $n_\delta = 1.7$ in Block B, which means that 3.0 grids distributed in Block A and 1.7 grids in Block B with the vertical dimension.

Since the most concerned area of the hydrodynamic aspect is the skimming tower, the majority of grids are concentrated inside the tower. The ratio of the number of grids

inside the tower to the total grids is $\frac{n_{Tower}}{n_{Total}} = 63.6\%$. Note that the geometry volume ratio between the tower and the whole computational domain is $\frac{V_{Tower}}{V_{Total}} = 16.4\%$. Hence, it is of importance to distribute more grids in the skimming tower to obtain the better solution of problems involving the three-phase flow interfaces.

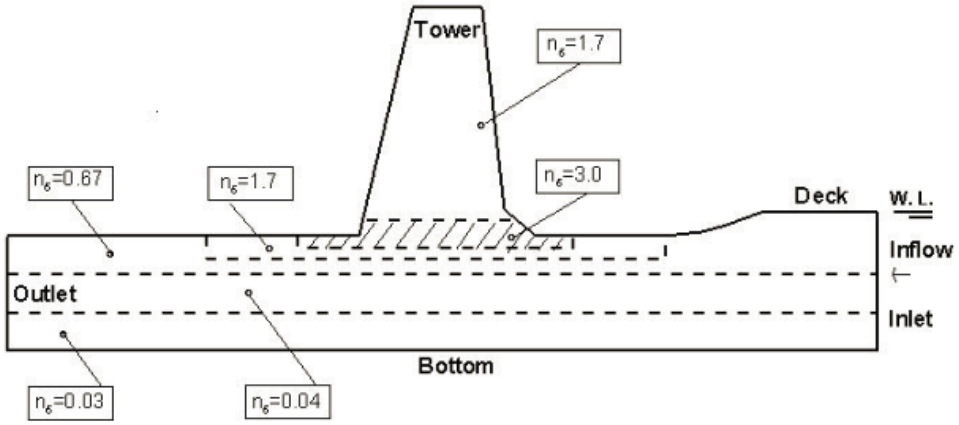

(a)

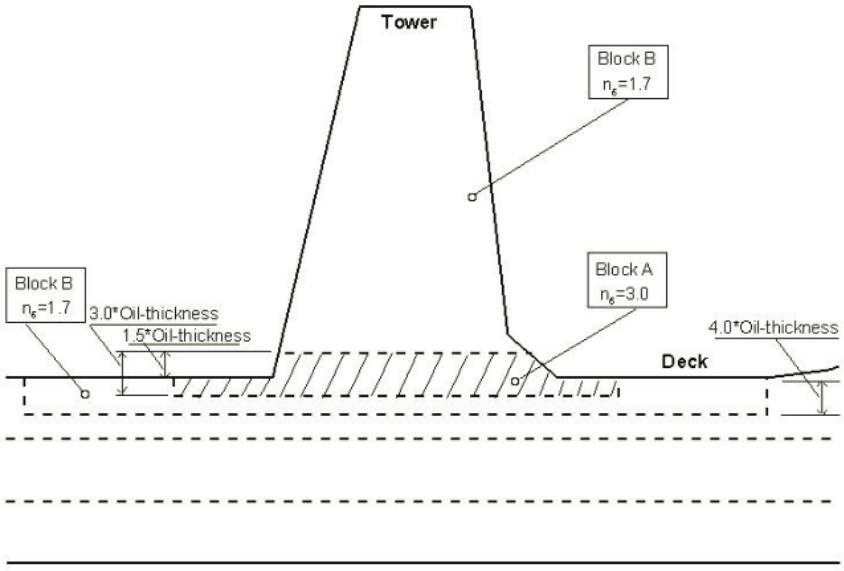

(b)

Figure 4.5 Schematic grid distribution for 16.2 million grids

Chapter 5

Simulation Results

The numerical simulation results are presented in this chapter, including the simulation conditions and the comparison of experimental results and numerical solutions. The numerical results obtained from the CFD simulation are able to validate the experimental data. The improvements of the numerical results are also discussed. In this chapter, the convergence studies are also presented. The four sets of mesh have been generated as well as the results are discussed and analysed.

5.1 Simulation Conditions

The CFD simulations were centered on the mesh with16.2 million grids. The total simulation time was 5.0 s. The oil skimmer was accelerating from $u_t = 0.0\ m/s$ to the constant service speed $u_t = 0.572\ m/s$. The simulation time was kept the same as the measured experimental time. The calculation of Courant numbers showed that the time step applied in the numerical simulation has to be equal to or smaller than 0.005 s. Therefore, the time step was chosen as $\Delta t = 0.005$ s. The number of inner iteration in the solver was set as 30. This conclusion is based on the theory of Courant numbers. The Courant numbers are defined as

$$C = \frac{u \cdot \Delta t}{\Delta x} \leq C_{max} \tag{5.1}$$

where u is the velocity of the vessel, Δt is the time step and Δx is the length interval.

The value of C_{max} is typically equal to1. The Courant number is dimensionless, where the time step must be less than a certain time in the explicit time-marching numerical simulations. If this requirement is not satisfied, the simulation is most likely to produce incorrect results. In order to keep the Courant number with the same value for other speeds, the time step, for example, was increased to $\Delta t = 0.01$ s for the case with $u_t = 0.216$ m/s.

5.2 Simulation Results

The snapshots of oil flow motion in the skimming tower obtained from the experiments which are at various time instants with an interval time of 1.0 s are presented below (Figures 5.1 to 5.5). The snapshots of the numerical results obtained from Star-CCM+ are also followed. They are compared with those taken in the experiments. The agreement between the experimental and numerical results is generally reasonable.

However, there are some discrepancies occurred between the numerical and experimental snapshots. Since the thickness of the oil slick was just 2.0 mm, it can be observed that the oil slick in the trim tank was not evenly spread. It is difficult to guarantee the thickness of the oil slick was maintained at the same level everywhere during the experiment. Whereas, the oil slick is defined as evenly distributed with uniform thickness in the numerical simulation. This may be one of the essential reasons that caused the discrepancy of flow patterns. The other reason for the discrepancy is likely due to the simplifications in the numerical model. The force induced from the oil skimmer might

need to be considered in the further investigation where the improved numerical model is conducted. In addition, it is always concluded that is the finer grids applied, the better result obtained. This problem will be discussed in the convergence studies section in which four sets of mesh have been investigated.

It can be seen that the discrepancy in Figure 5.2 is more significant than other figures. The most possible impact to cause this discrepancy is due to the acceleration of the skimmer. Hence, the acceleration can be investigated and improved in the further study.

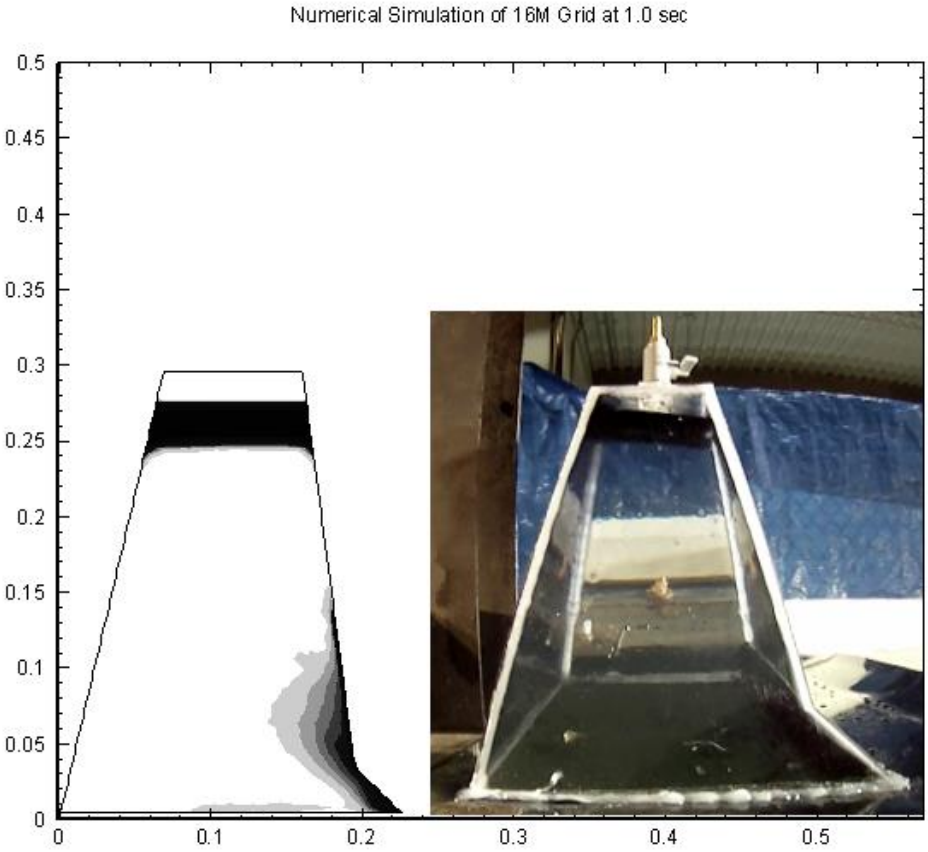

Figure 5.1 Comparison of experimental and numerical snapshots at t=1.0 s

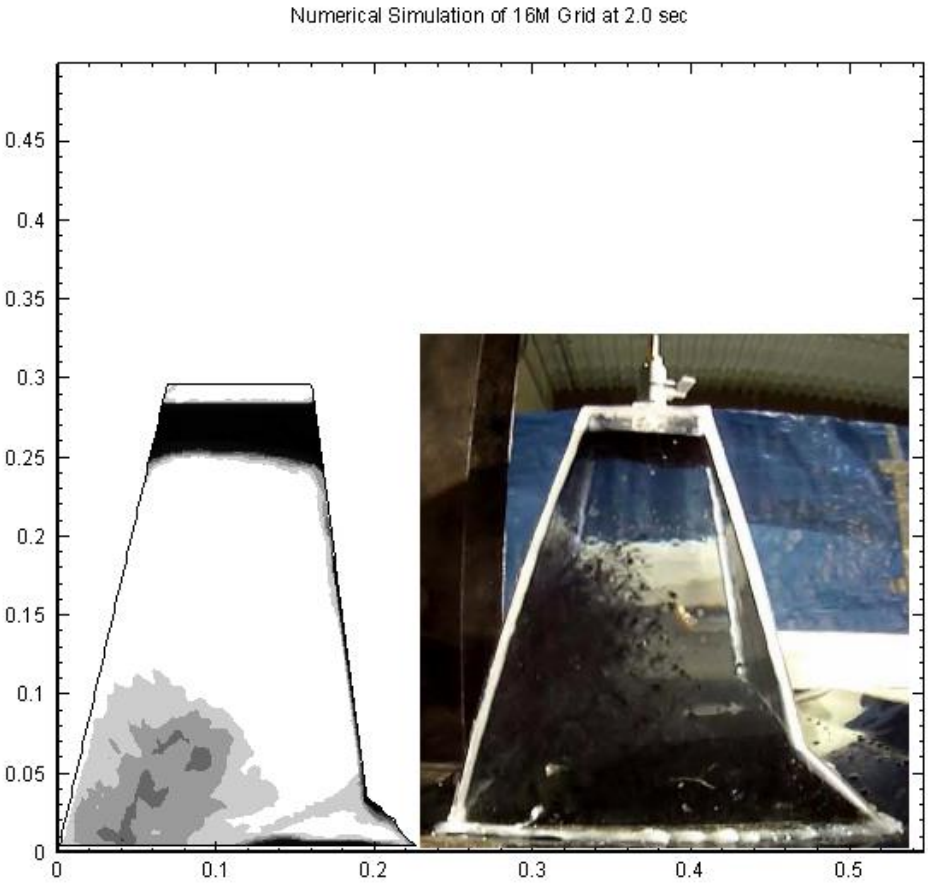

Figure 5.2 Comparison of experimental and numerical snapshots at t=2.0 s

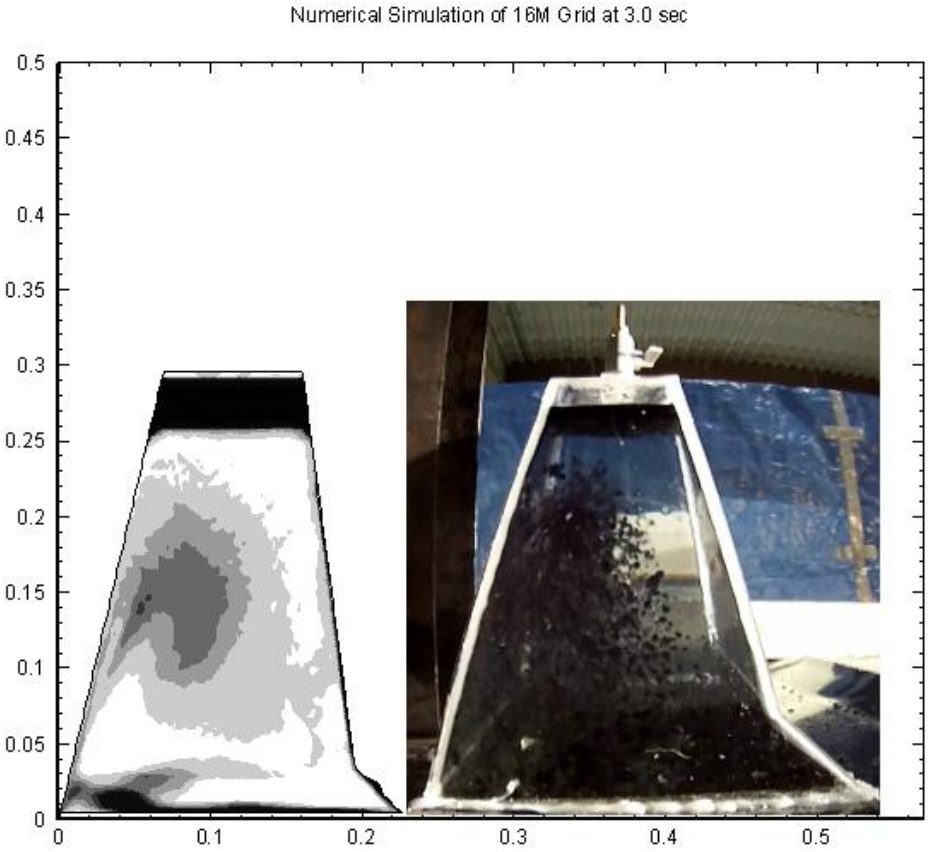

Figure 5.3 Comparison of experimental and numerical snapshots at t=3.0 s

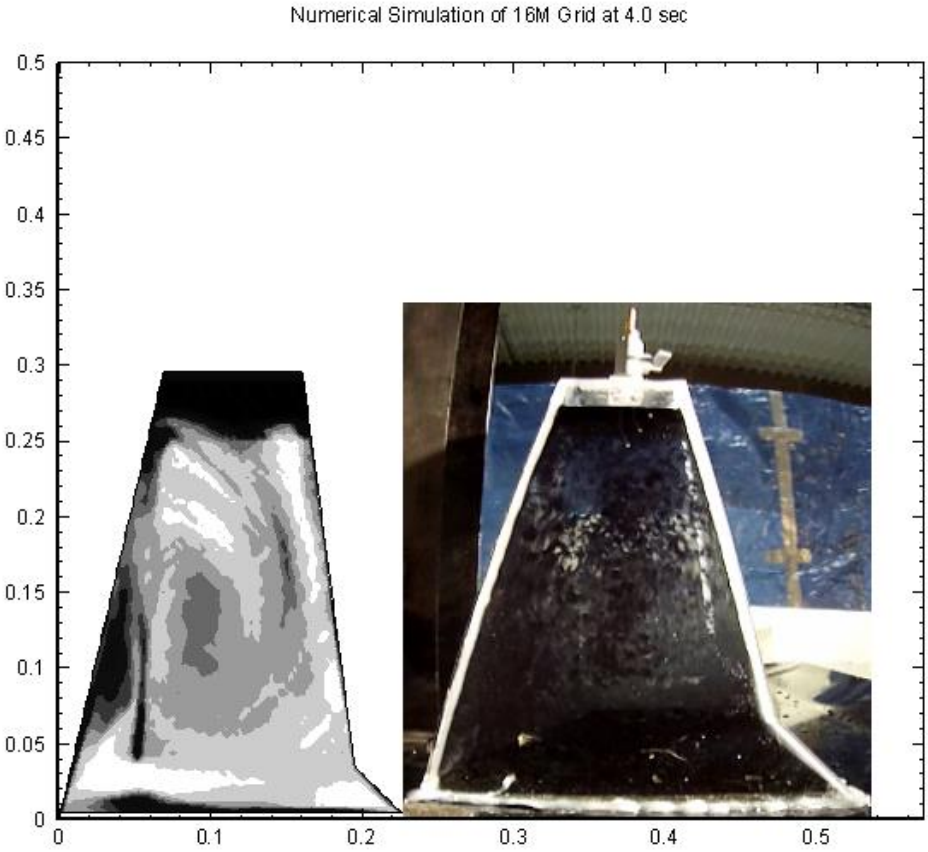

Figure 5.4 Comparison of experimental and numerical snapshots at t=4.0 s

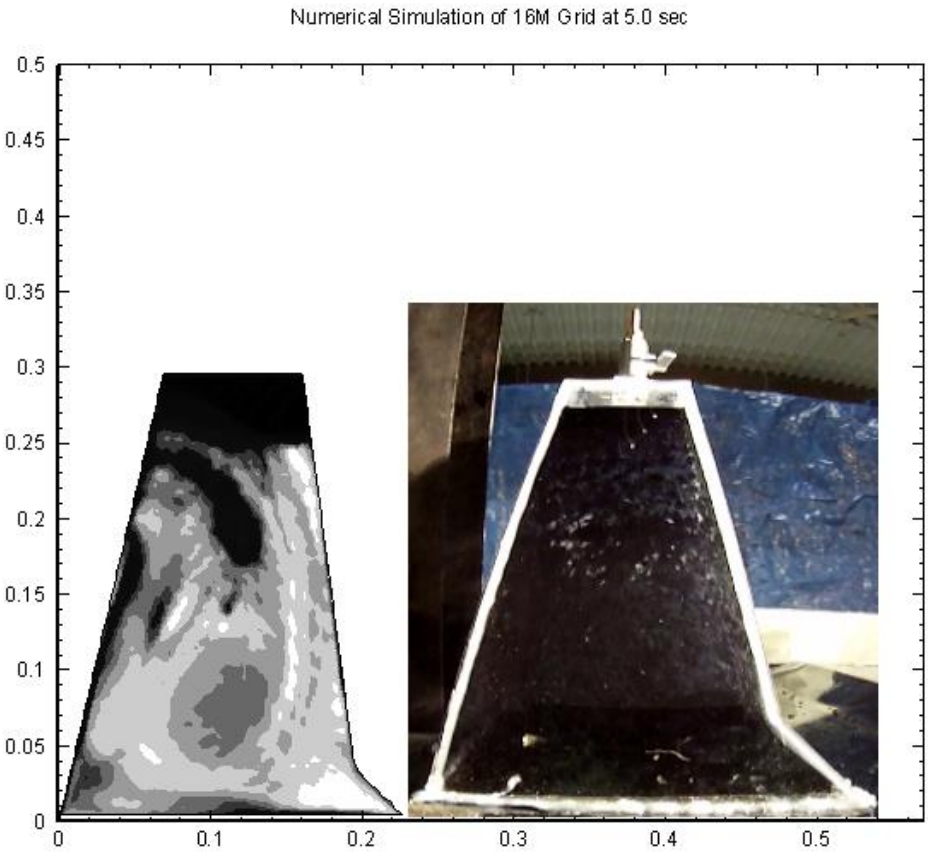

Figure 5.5 Comparison of experimental and numerical snapshots at t=5.0 s

5.3 Numerical Analysis

The volume of skimmed oil in the tower can be obtained, and non-dimensionalized based on the below equation. The value is calculated from the volume of skimmed oil divided by the volume of tower. In Figure 5.6, the non-dimensional value is plot against the time and the travelled distance of the oil skimmer.

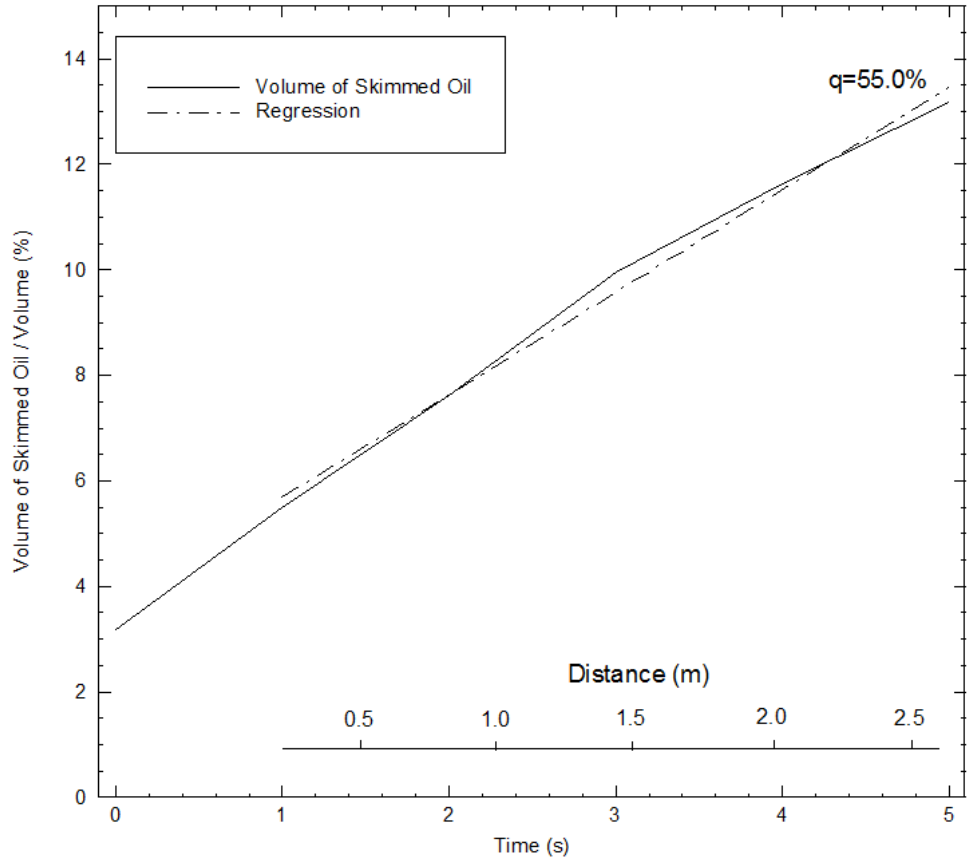

Figure 5.6 Computed volume of skimmed oil in the tower at speed of $0.527\ m/s$ against time and travelled distance

The computed volume of skimmed oil can be introduced based on the above figure, assuming the skimmed fluid was pure oil,

$$\sigma = \frac{V_{SkimmedOil}}{V_{Tower}} \tag{5.2}$$

where σ is the nondimensionalized value, $V_{SkimmedOil}$ is the volume of skimmed oil in the tower, V_{Tower} is the volume of tower.

It can be observed in the Figure 5.6 that the non-dimensional oil skimmed volume has a roughly linear curve versus the travelled time t or distance x when $t > t_0$. In order to analyse the relationship between the skimming performance of the oil skimmer and the travelled time t or distance x, a regression line with a slope, S, is introduced by using the least square method.

$$\sigma = \frac{V_{SkimmedOil}}{V_{Tower}} = Sx + b \tag{5.3}$$

In this case, the volume of skimmed oil in the tower can be expressed below,

$$V_{SkimmedOil} = V_{Tower} \cdot (Sx + b) \tag{5.4}$$

then it can have the derivation of the volume of skimmed oil to the travelled distance. Hence, the volume of skimmed oil recovered in the tower per unit travelled distance, Q, can be obtained,

$$Q = \frac{dV_{SkimmedOil}(x)}{dx} = V_{Tower} \cdot S \tag{5.5}$$

With the expression of the volume of skimmed oil into the tower per unit distance, the recovery rate, q, can be defined, and can applied to investigate the recovery efficiency.

The recovery rate is equal to the volume of skimmed oil in the tower per unit distance divided by the total volume of oil in the base of the tower.

$$q = \frac{Q}{Q_0} = \frac{SV_{Tower}}{\delta_{Oil} B_{Tower}} \tag{5.6}$$

where B_{Tower} is the width of the base of the tower, q is the non-dimentional recovery rate.

It can be concluded that, based on the equation of the recovery rate, the ideal case is when $q = 1$. That means all the oil underneath the tower will be skimmed into the tower. The studies of oil skimmer geometry optimization are mainly concentrated on modifying the two variants, V_{Tower}, and B_{Tower}, to improve the recovery efficiency. The details of the optimization will be discussed in the next chapter.

5.4 Convergence Studies

There were four sets of mesh generated and employed in the convergence studies. Table 5.1 presents the number of grids used in these four sets of mesh, and the number of grids in two significant volume mesh modified by the variable, n_δ, which has been defined in the section of grid generation. In Figure 4.5, it is observed that the volume mesh in the computational domain can be separated into two kinds of blocks with different grids density, i.e., Block A and Block B. The grids distribution were kept the same for the four

sets of mesh, while n_δ was varied in different cases. The values of n_δ with four sets of grids in Block A and Block B can be seen in Figure 5.7 (A) to (D).

Table 4.1 List of Grids Used in the Convergence Studies

		Grid-1	Grid-2	Grid-3	Grid-4
Grid number (Million)		21.0	16.2	11.4	7.3
Grid number, n_δ, in an oil layer with thickness of 2.0mm	Block A	3.0	3.0	1.7	2.5
	Block B	2.2	1.7	1.7	1.2

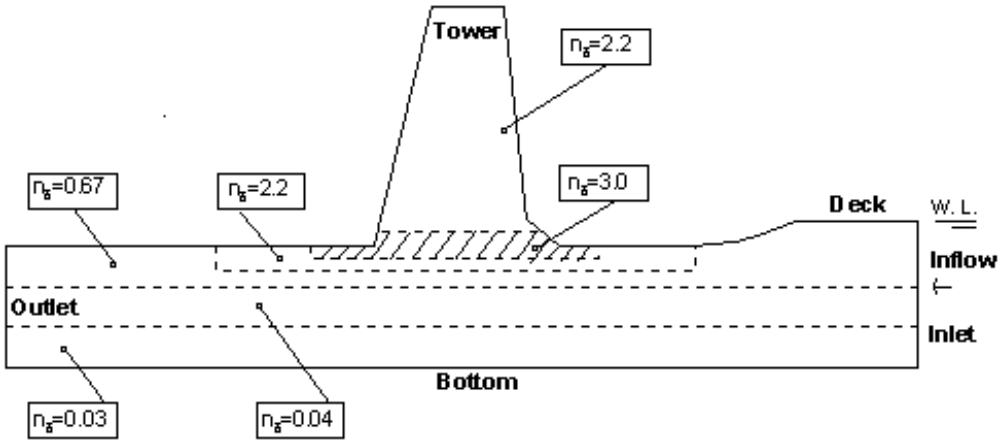

(A) Grid-1 with 21 million grids

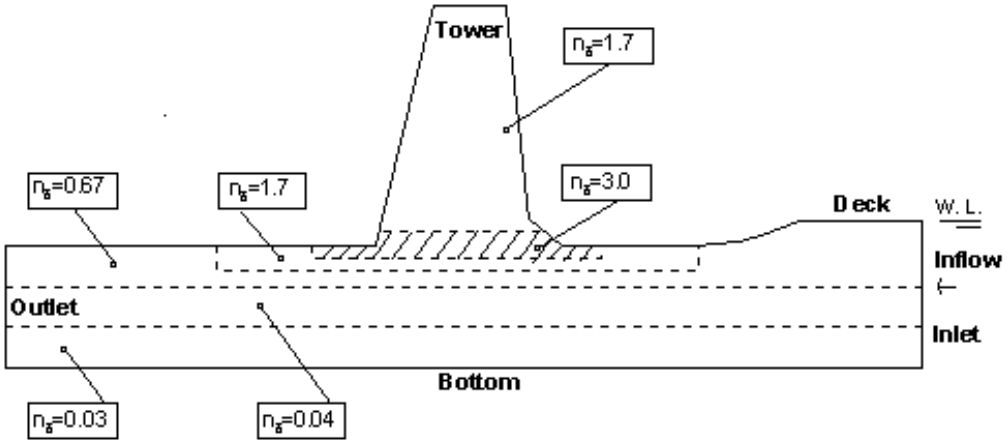

(B) Grid-2 with 16.2 million grids

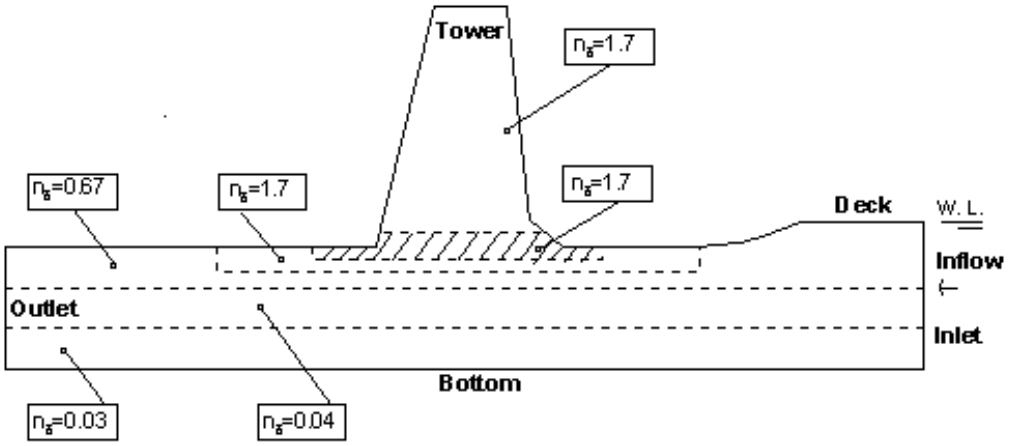

(C) Grid-3 with 11.4 million grids

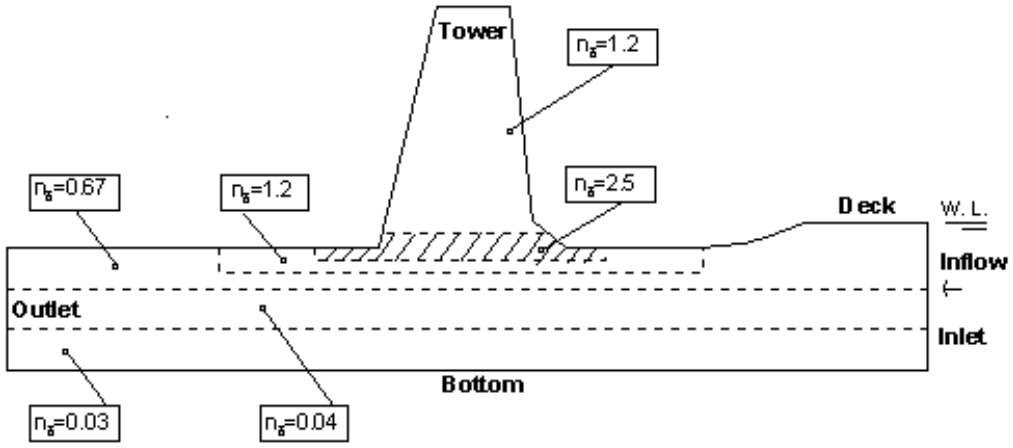

(D) Grid-4 with 7.3 million grids

Figure 5.7 Different n_δ values with four sets of grids

Grid-1 is the finest grid considering the current computer capabilities, while Grid-4 is the coarsest grid. The comparison of snapshots from the four sets of mesh at various time instants (from $t = 1.0\ s$ to $t = 5.0\ s$) with an interval of $1.0\ s$ are presented in the following figures (Figures 5.8 to 5.12). These figures shows that the flow patterns in the tower are mostly similar among the four sets of grids. However, the slight discrepancies are still existed. Comparing to the experiments snapshots, Grid-4 with the coarsest grid has the worst solution for the vortex of the fluid mixture. Grid-1 and Grid-2 have the similar results that are most agreeable witht those from the experiments. Considering the calculation cost efficiency and the computing power, Grid-2 with 16.2 million grids would be prefered.

(a) Grid-1

(b) Grid-2

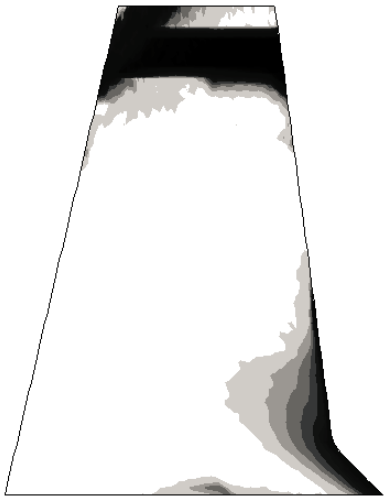

(c) Grid-3

(d) Grid-4

Figure 5.8 Comparison of oil flow patterns at $t = 1.0\ s$ for four sets of mesh

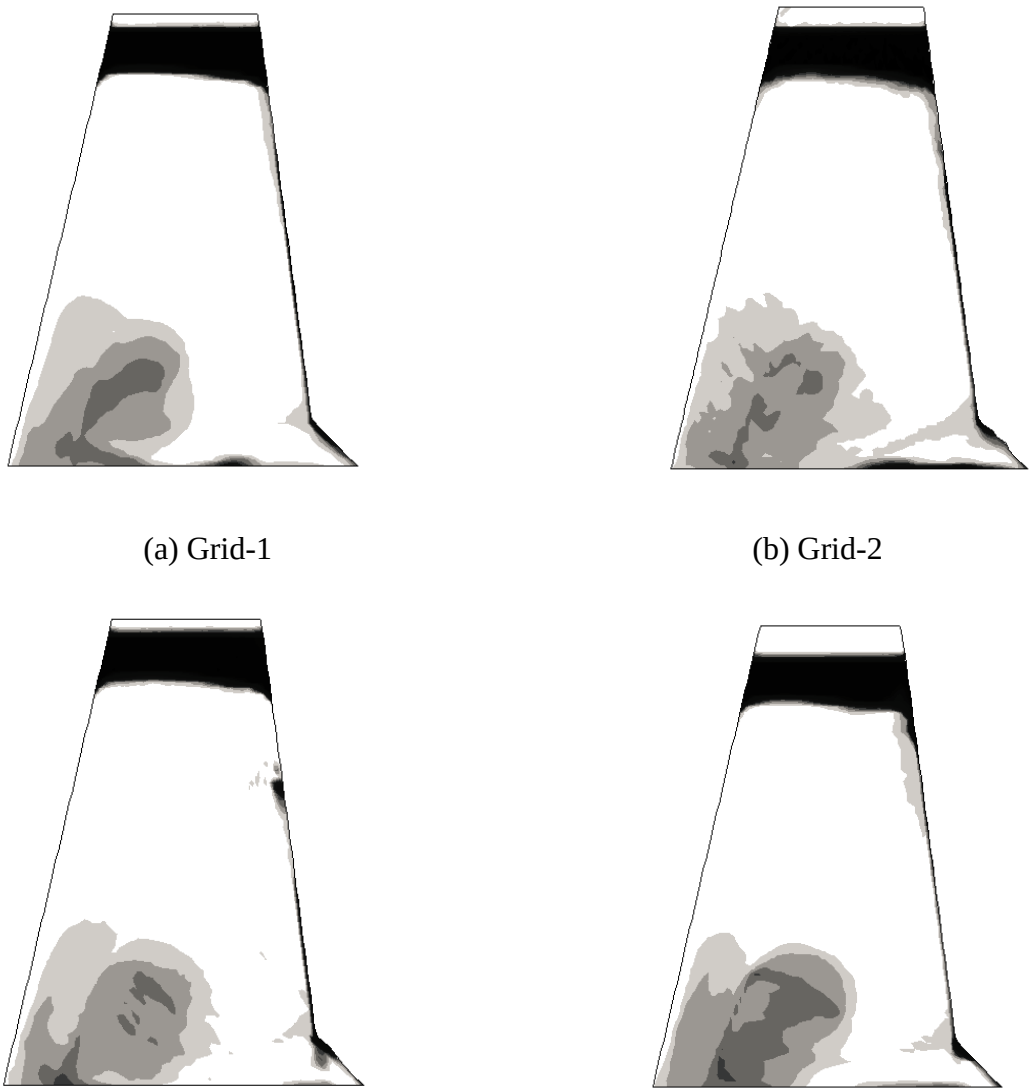

(a) Grid-1 (b) Grid-2

(c) Grid-3 (d) Grid-4

Figure 5.9 Comparison of oil flow patterns at $t = 2.0\ s$ for four sets of mesh

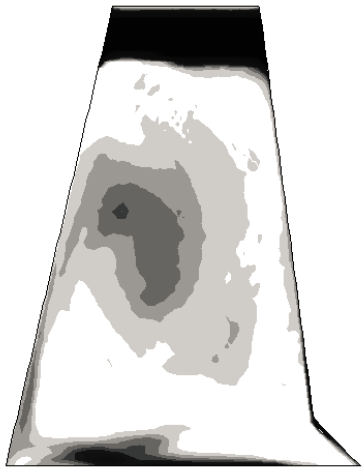

(a) Grid-1

(b) Grid-2

(c) Grid-3

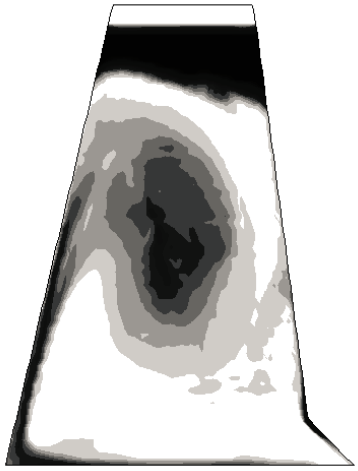

(d) Grid-4

Figure 5.10 Comparison of oil flow patterns at $t = 3.0\ s$ for four sets of mesh

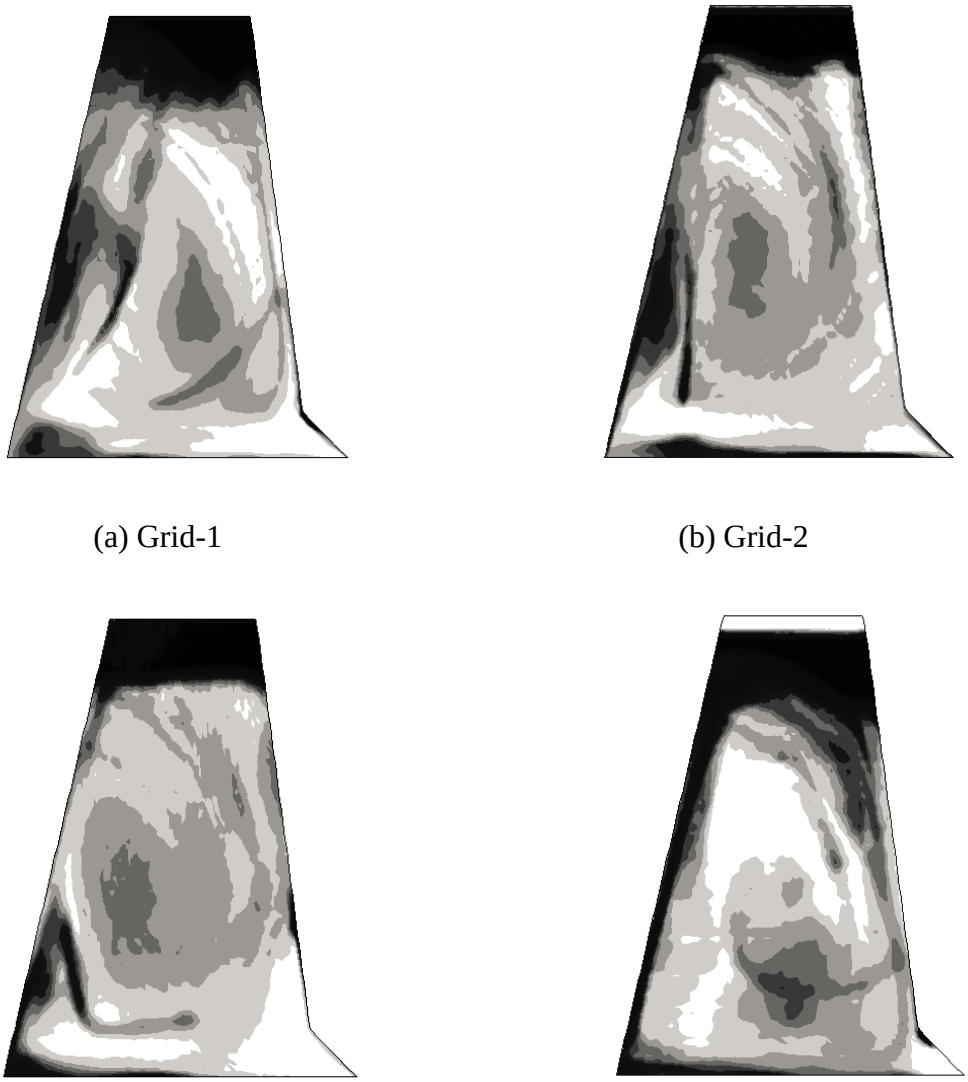

(a) Grid-1 (b) Grid-2

(c) Grid-3 (d) Grid-4

Figure 5.11 Comparison of oil flow patterns at $t = 4.0\ s$ for four sets of mesh

(a) Grid-1

(b) Grid-2

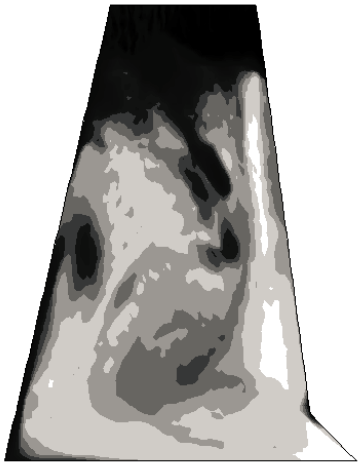

(c) Grid-3

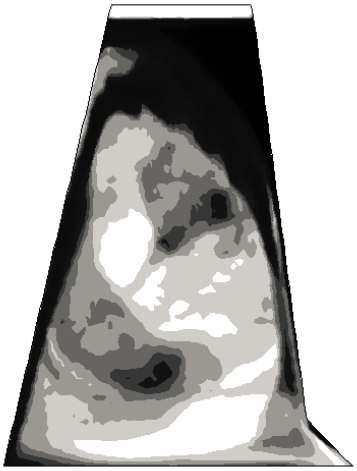

(d) Grid-4

Figure 5.12 Comparison of oil flow patterns at $t = 5.0\ s$ for four sets of mesh

Figure 5.13 presents the comparison of the ratio, σ, where $\sigma = \frac{V_{SkimmedOil}}{V_{Tower}}$, against the travelled time t obtained from the four sets of mesh. The difference of the ratios among Grid-1, Grid-2 and Grid-3 is insignificant, while Grid-1 and Grid-2 have better agreement

with the experimental results on the oil droplet captures. Base on the principle of convergence studies, Grid-2 is the most appropriate selection due to precise numerical prediction along with time and power cost efficient. Therefore, Grid-2, with the number of grids is 16.2 million, will be used in the optimization studies.

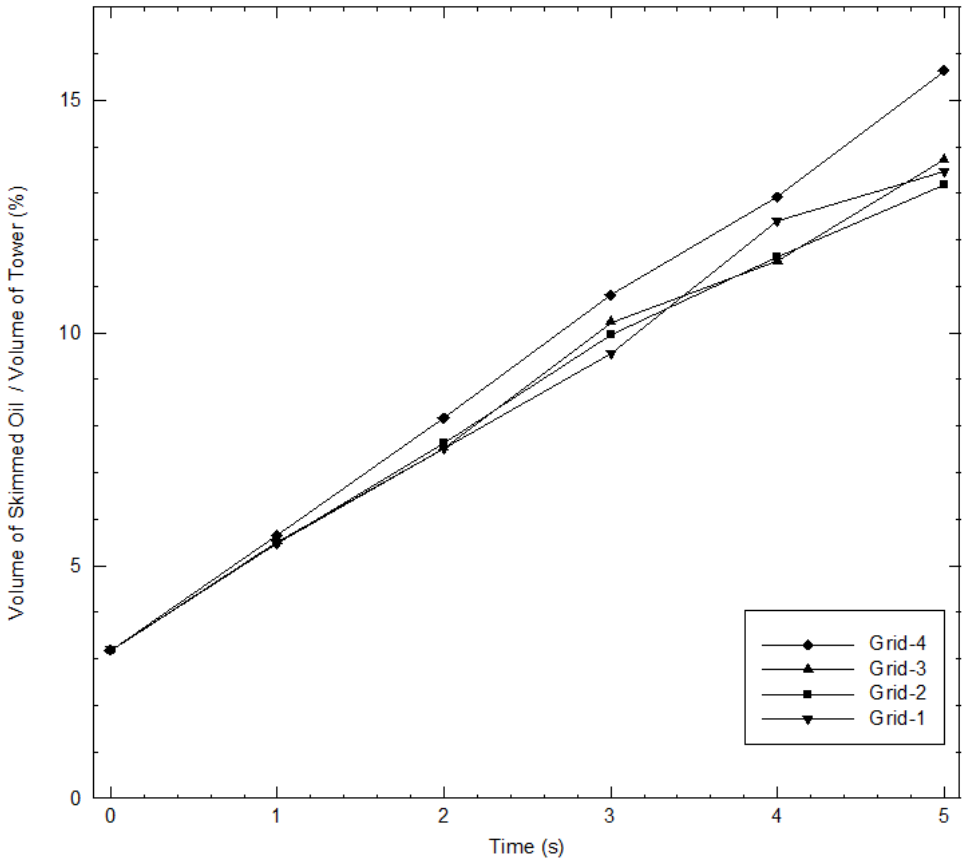

Figure 5.13 Computed volume of skimmed oil for four sets of mesh

It can be also concluded from the convergence studies that the grid size in the entire tower must be sufficiently small because many small oil drops were formed in the oil skimming process. The snapshots from the experimental results have already shown the effects of small oil drops during the skimming process. The analysis of oil drop size can be carried out in the future work. The relationship between grid size and oil drop size will also be investigated.

Chapter 6

Optimization

Optimization studies were carried out to select optimal tower geometry for higher recovery rate q, which were predicted by CFD software. The effect of the service speed on the recovery efficiency was also investigated. The experimental data with optimal advancing speed are employed to compare with the numerical results in this section. Grid-2 with a total of 16.2 million grids were used in the simulations.

6.1 Optimization of Tower Geometry

The basic principle to optimize the skimming tower geometry can be according to the equation to calculate the recovery rate, $q = \frac{Q}{Q_0} = \frac{SV_{Tower}}{\delta_{Oil} B_{Tower}}$, where to increase the volume of the tower and/or to decrease the width of the base of the tower may improve the recovery efficiency. Based on this conclusion, there is an improved tower geometry that can be introduced immediately. To increase the volume of the tower by extending the length of the tower base can be considered as the first option to improve the recovery rate, which is denoted as Optimal_1. Figure 6.1 (a) showed the oil flow pattern and the velocity field of the tower with the original geometry at time instant 6.0 s. It can be seen that a clockwise vortex occurs in the tower that drives the oil to rise on the back wall and slip along the front wall. As observed from this figure, another improved tower geometry to increase the oil recovery rate can be achieved by modifying the back wall slope to ease the rise-up of the oil, while the length of the tower base were kept the same. This means

that more recovered and rise-up oil will be remained in the tower while be getting difficult to slip downward. This optimization of tower geometry is denoted as Optimal_2.

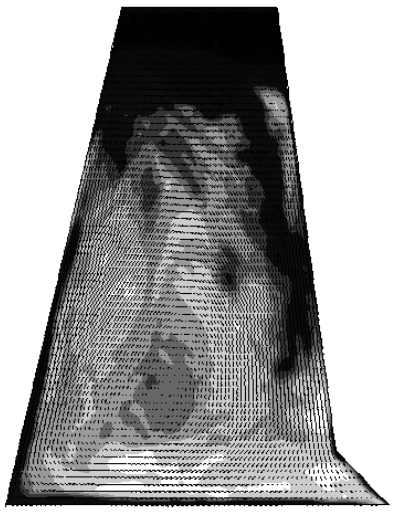

(a) Original

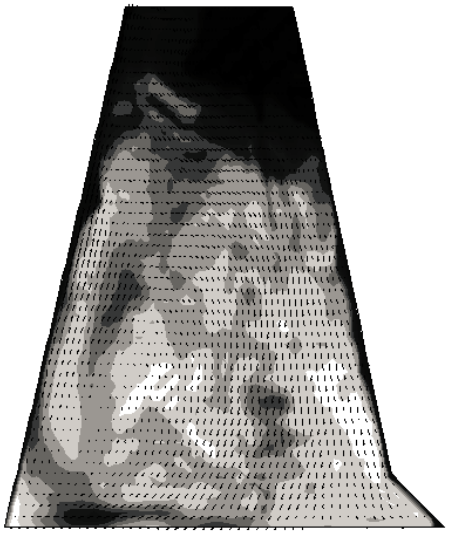

(b) Optimal_1

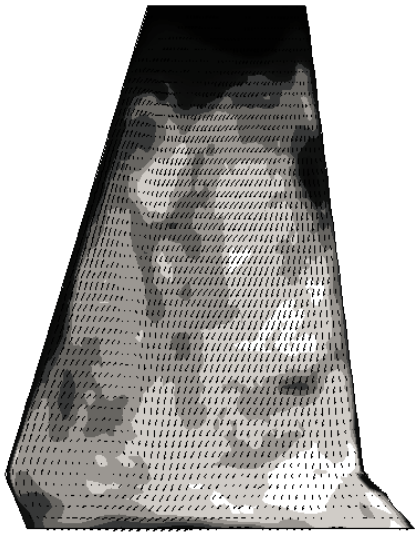

(c) Optimal_2

Figure 6.1 Comparison of oil flow patterns obtained from different tower geometries at time instant $6.0\ s$ (arrows represent the velocity vectors)

6.1.1 First Optimization of Tower Geometry (Optimal_1)

The length of tower base, L_{Tower}, can be extended. As discussed above, this modification is to increase the volume of the tower. It is also to allow oil underneath the tower to have sufficient time to rise into the tower. In order to test the efficiency with the optimized geometry, an example with lengthened tower length has been generated. The case with the length of the tower base extended from 23.0 to 30.0 mm forward, which was 13% increased in the tower base area, was investigated in Star-CCM+. Figure 6.1 (b) shows the pattern of the oil flow in the tower and the comparison of the tower geometry with the original one. The snapshots of the oil flow pattern obtained from the numerical simulation

with the time interval of 1.0 s starting from 1.0 s to 10.0 s are presented in Figure 6.2. It also can be seen in Figure 6.3 (A) that Optimal_1 is able to skim more oil than the original one especially after 5.0 sec. Figure 6.3 (B) and (C) compare the snapshots of the oil flow patterns of the original model and the Optimal_1 model at 5.0 sec and 10.0 sec.

(1) $t = 1.0\ s$ (2) $t = 2.0\ s$

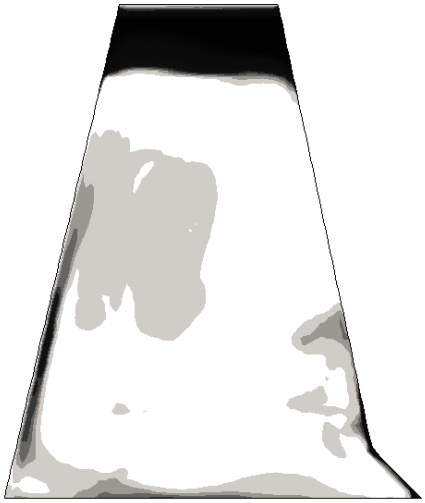

(3) $t = 3.0\ s$

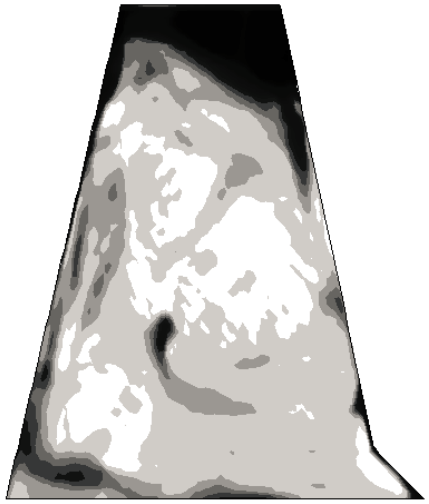

(4) $t = 4.0\ s$

(5) $t = 5.0\ s$

(6) $t = 6.0\ s$

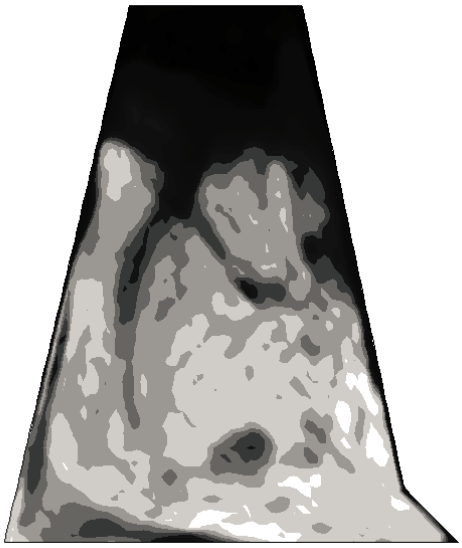

(7) $t = 7.0\ s$

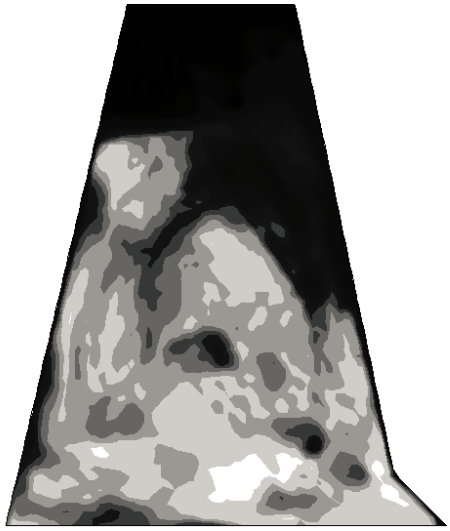

(8) $t = 8.0\ s$

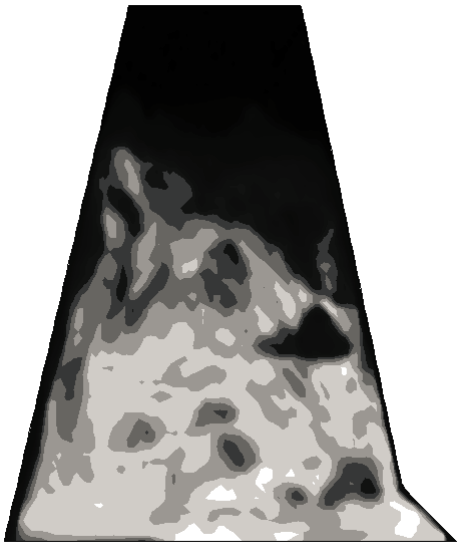

(9) $t = 9.0\ s$

(10) $t = 10.0\ s$

Figure 6.2 Oil flow patterns with Optimal_1 geometry at various time instants

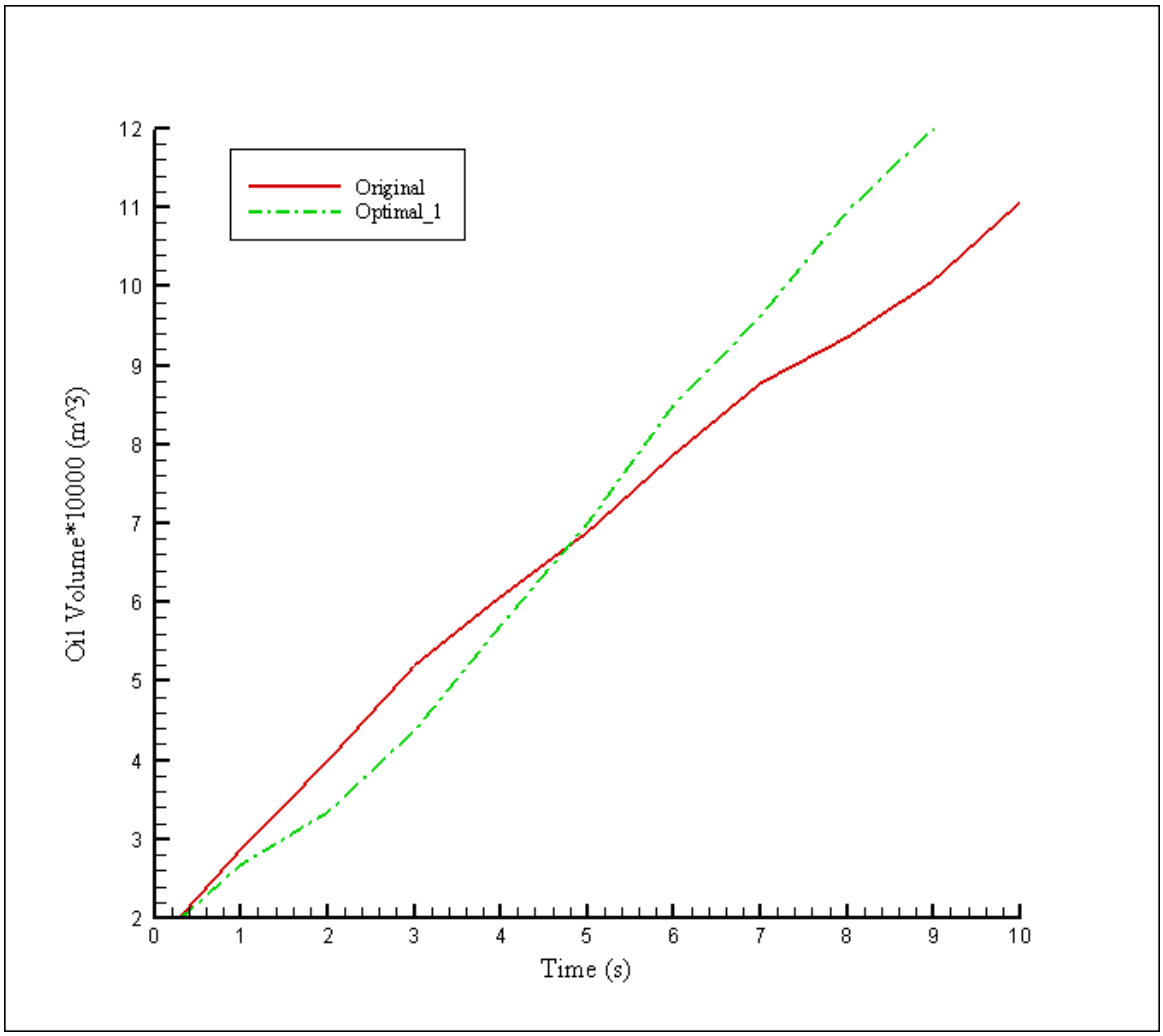

Figure 6.3 (A) Computed volume of skimmed oil with the original geometry and Optimal_1 geometry

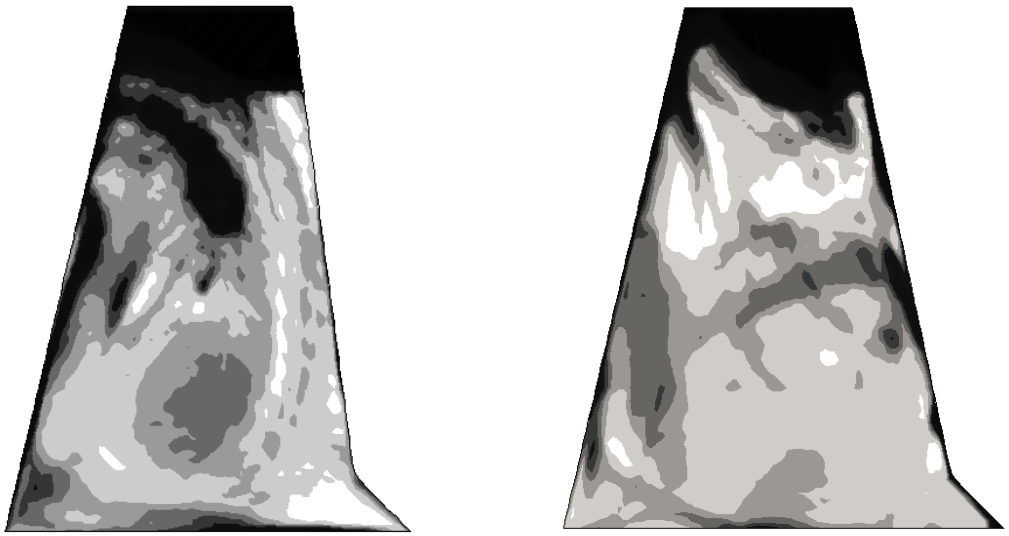

Original Optimal_1

Figure 6.3 (B) Comaparison of the oil flow patterns of the original model and the Optimal_1 model at 5.0 sec

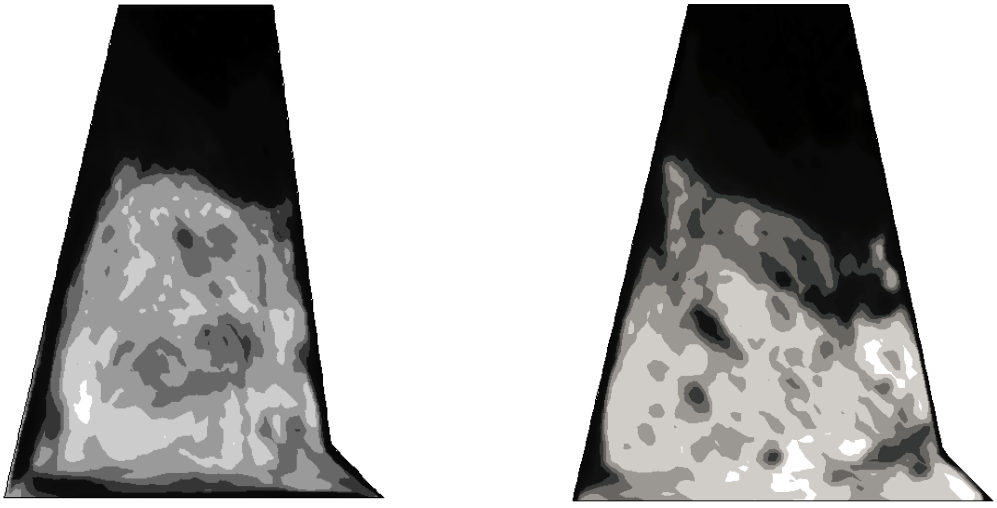

Original Optimal_1

Figure 6.3 (B) Comaparison of the oil flow patterns of the original model and the Optimal_1 model at 10.0 sec

6.1.2 Second Optimization of Tower Geometry (Optimal_2)

The second optimization is focused on the angle between the rear surface and the horizontal plane, which can be increased to facilitate the oil flow to enter into the tower and to rise up easily. In order to investigate the effects of the recovery rate caused by this change, an example with the angle increased from $75°$ to $120°$ was conducted in Star-CCM+. Note that the length of the tower base in this case was kept as same as the original one. Figure 6.1 (c) shows that the oil accumulation in the back corner is reduced compared with it in the original one, while less oil is moved downward the front wall. It can be also observed that Figure 6.1 (c) shows the change of the tower geometry compared to the original design. The snapshots of the oil flow pattern obtained from the numerical simulation with the time interval of $1.0\ s$ starting from $1.0\ s$ to $10.0\ s$ are presented in Figure 6.4.

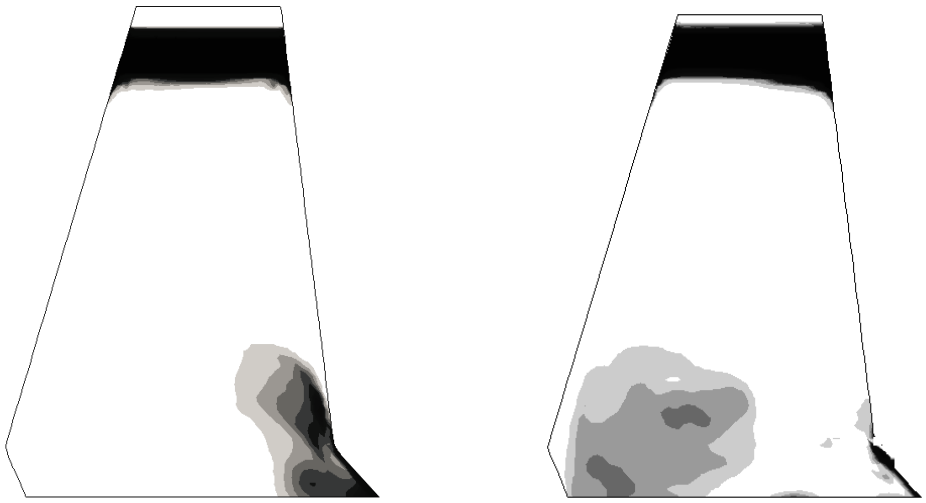

(1) $t = 1.0\ s$ (2) $t = 2.0\ s$

(3) $t = 3.0\ s$

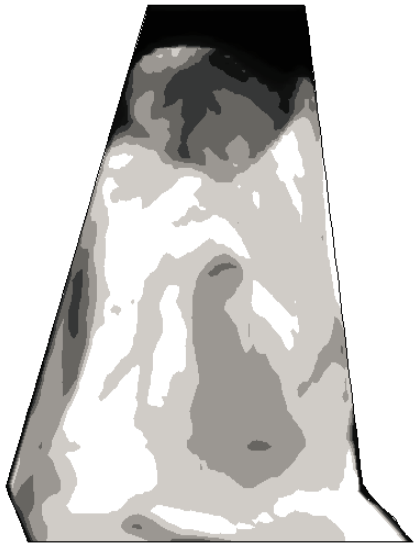

(4) $t = 4.0\ s$

(5) $t = 5.0\ s$

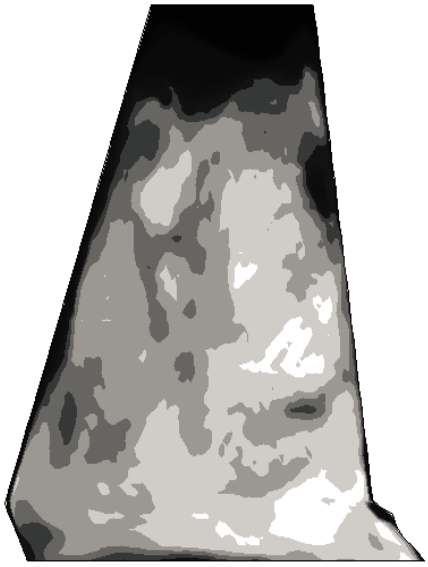

(6) $t = 6.0\ s$

(7) $t = 7.0\ s$

(8) $t = 8.0\ s$

(9) $t = 9.0\ s$

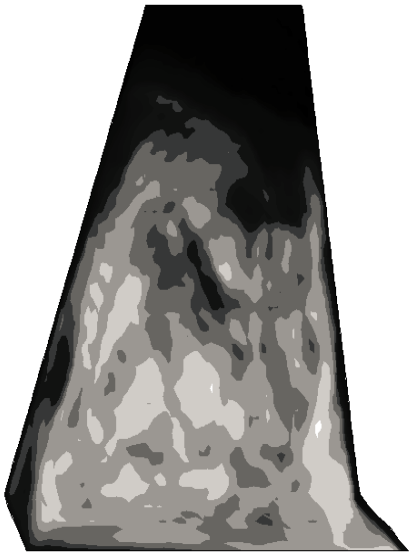

(10) $t = 10.0\ s$

Figure 6.4 Oil flow patterns with Optimal_2 geometry at various time instants

Figure 6.5 presents the computed volumes of skimmed oil for the original one, Optimal_1, and Optimal_2. Since the volumes of the tower among these three tower geometries are different (Table 6.1), it is more straight forward to apply the actual volumes of skimmed oil instead of using the recovery efficiency rate for the comparison. Figure 6.5 shows that Optimal_1 is more effective than the original one and Optimal_2 after $5.0\ sec$. This means that it takes less time for Optimal_1 to recover the same volume of oil. With respect to the comparion of the recovery rates, Optimal_1 has 65.8% and Optimal_2 has 51.5%, while the original model has 48.1%. Hence, the improvement by Optimal_1 has more significant effect on recovering oil than that by Optimal_2. This can be concluded that to increase the length of the base tower is more effective than modifying the back wall geometry. Figure 6.5 (B) and (C) compare the snapshots of the oil flow patterns of the original model, the Optimal_1 model and the Optimal_2 model at 5.0 sec and 10.0 sec.

Table 6.1 Volumes of three different tower geometries (m^3)

Original Geometry	0.523×10^{-2}
Optimal_1 Geometry	0.569×10^{-2}
Optimal_2 Geometry	0.569×10^{-2}

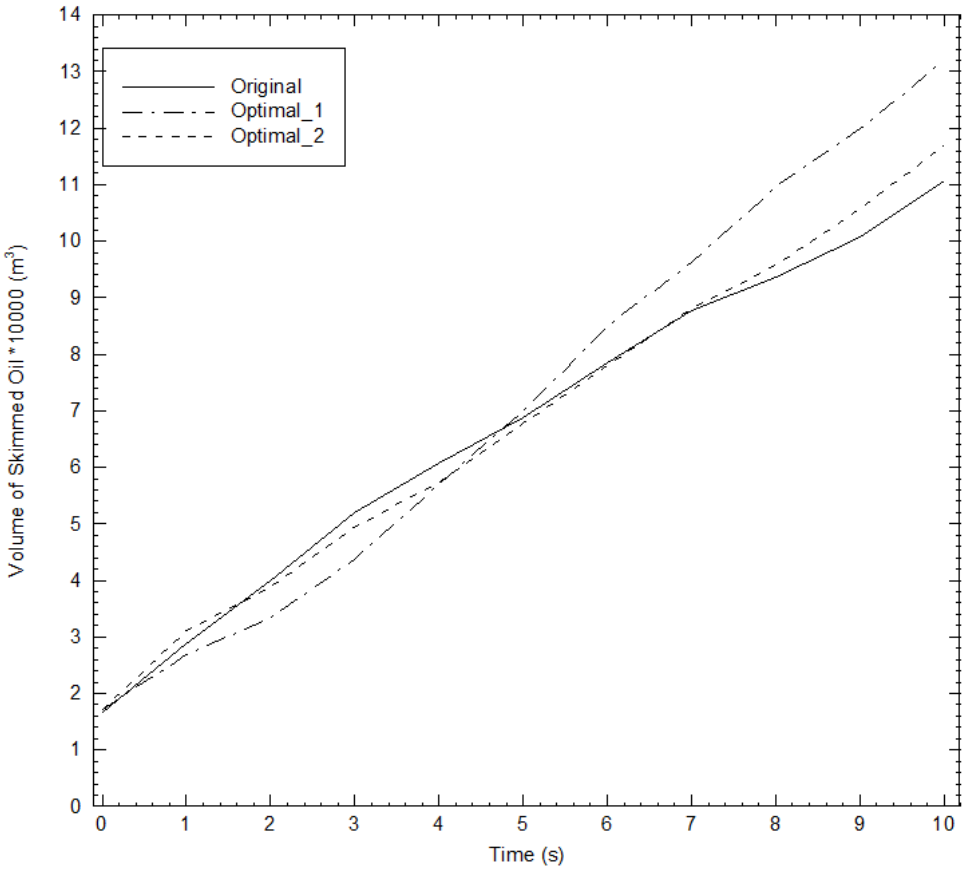

Figure 6.5 Computed volume of skimmed oil with three different geometries

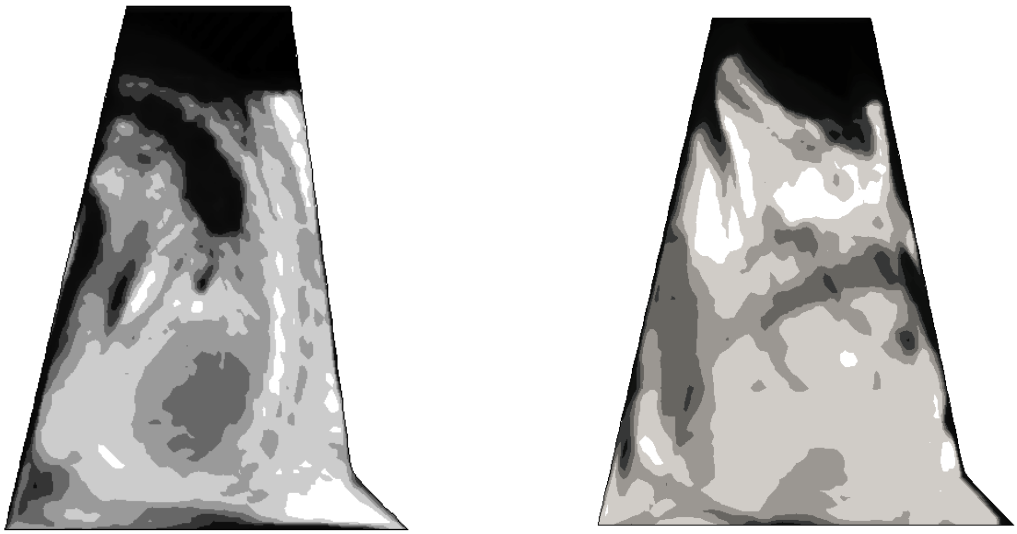

Original

Optimal_1

Optimal_2

Figure 6.5 (B) Comaparison of the oil flow patterns of the original model, the Optimal_1 model and the Optimal_2 model at 5.0 sec

Original

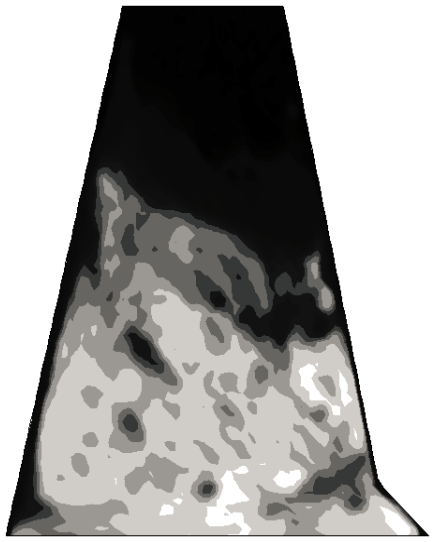

Optimal_1

Optimal_2

Figure 6.5 (B) Comaparison of the oil flow patterns of the origianl model, the Optimal_1 model and the Optimal_2 model at 10.0 sec

6.2 Optimization of Service Speed

The case with the optimized service speed was conducted both numerically and experimentally. It is always expected that the oil skimmer travelling with the lower speed can allow more oil underneath the base tower to have sufficient time to flow into the tower. However, it obviously has a limited lower speed for the skimmer. The lowest speed would need to be investigated in the future. In this case, the example of applying lower speed to the oilskimmer was carried out. In order to investigate the improvement by modifying the travelled speed, a lower service speed, $u_0 = 0.216\ m/s$, was introduced. This speed is corresponding to the Froude's number, $Fn = 0.051$, for the catamaran. The acceleration time is also set to $t_0 = 1.0\ s$.

The recovery efficiency rates, q, at two service speeds are presented in Figure 6.6. The horizontal axis is the travelled distance instead of travelled time, where the comparison of two service speeds travelling in the same distance is more straight forward and meaningful. It can be seen in Figure 6.6 that the recovery rate of the oil skimmer with the lower speed is apparently greater. In addition, since the same tower geometries were used in the numerical simulation, the recovery rate can be applied in the plot for the direct comparison.

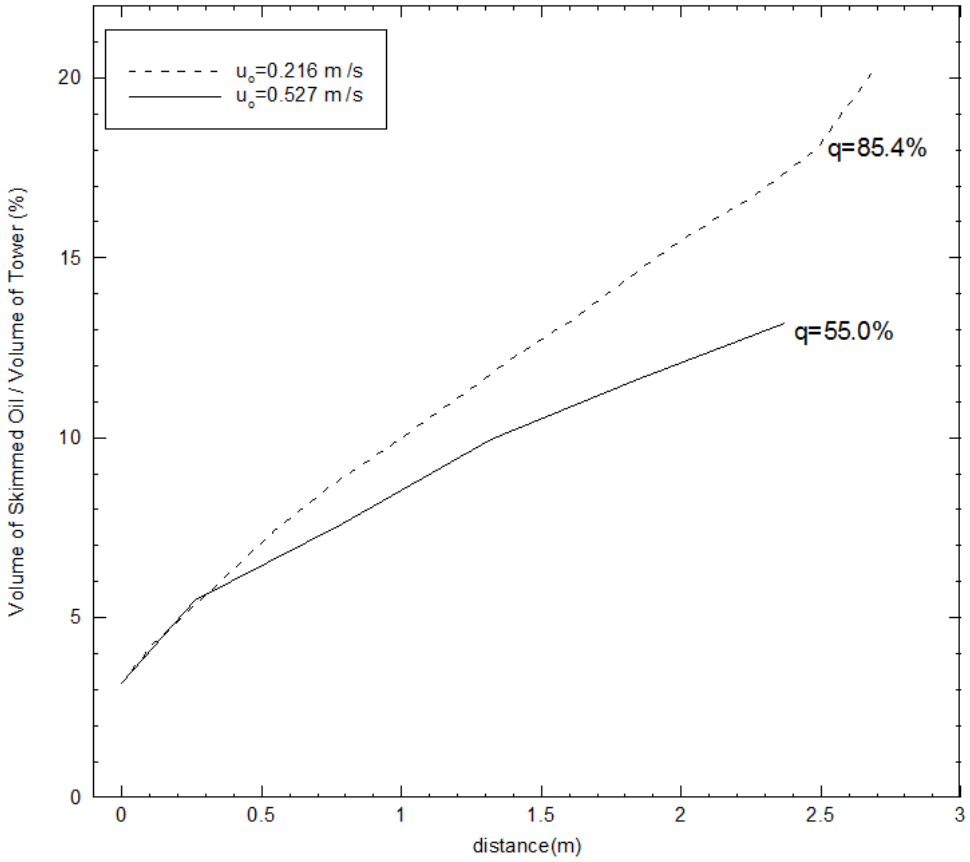

Figure 6.6 Computed volume of skimmed oil at two service speeds

Figure 6.6 shows the comparison of the oil flow patterns for the two speeds. These two flow patterns were captured at the time instant when the same distance, 2.37 m, was travelled, i.e., $t_0 = 5.0\ s$ for $u_0 = 0.527\ m/s$ and $t_0 = 11.5\ s$ for $u_0 = 0.216\ m/s$. They are also the final condition for both cases with two service speeds. The colors used in the figures are black and white where black represents oil and white represents water. There are some contours occurred that indicates the fluid mixture exists. It can be

observed in Figure 6.7 that more oil was skimmed at the lower speed than at the higher speed after travelling the same distance. In addition, the differences in the upper level of the skimming tower can be seen between two different approaching speeds. The snapshots with the velocity of $0.216\ m/s$ are more agreeable than those with the greater velocity. Prior to investigate the optimized speed for the oil skimmer model, the model with $0.527\ m/s$ can be considered as a low speed case so that the numerical model for incompressible air was reliable. However, the final results indicate that the numerical model for incompressible air works better in the lower speed case. This could be the main reason that leads the discrepancies between the numerical results and the experimental snapshots with the higher speed case.

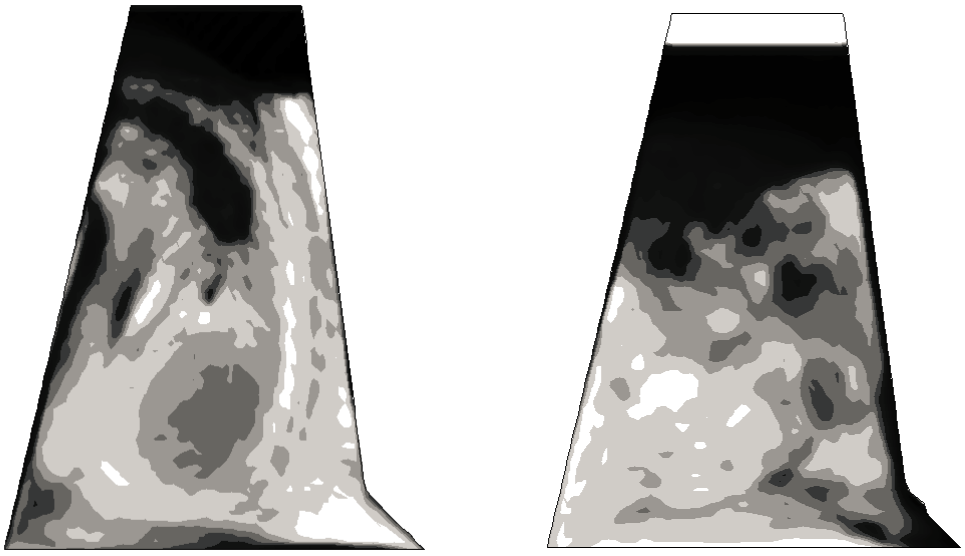

(a) $t = 5.0\ s$ and $u_0 = 0.527\ m/s$ (b) $t = 11.5\ s$ and $u_0 = 0.216\ m/s$

Figure 6.7 Comparison of oil flow patterns at two service speeds and at the same travelled distance

Figure 6.8 also presents the snapshots of the oil flow patterns from both the experiment and the numerical simulation with the time interval of $1.0\ s$ (starting from $1.0\ s$ to $13.0\ s$).

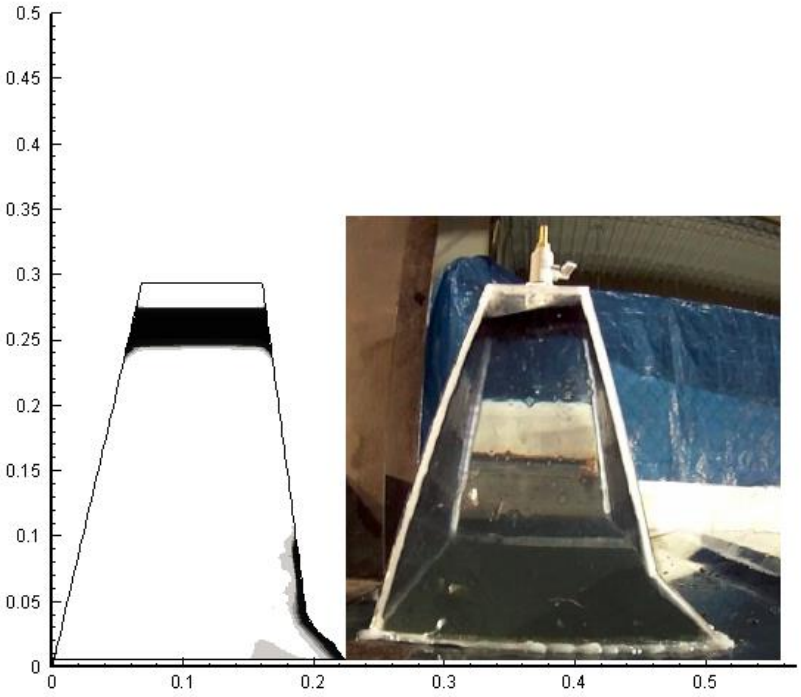

(1) Time instant=1.0 *s*

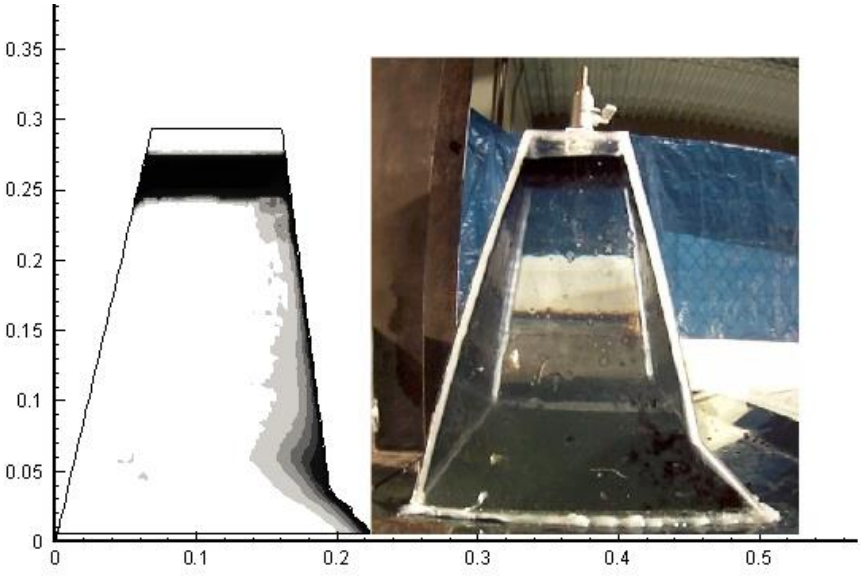

(2) Time instant=2. 0 *s*

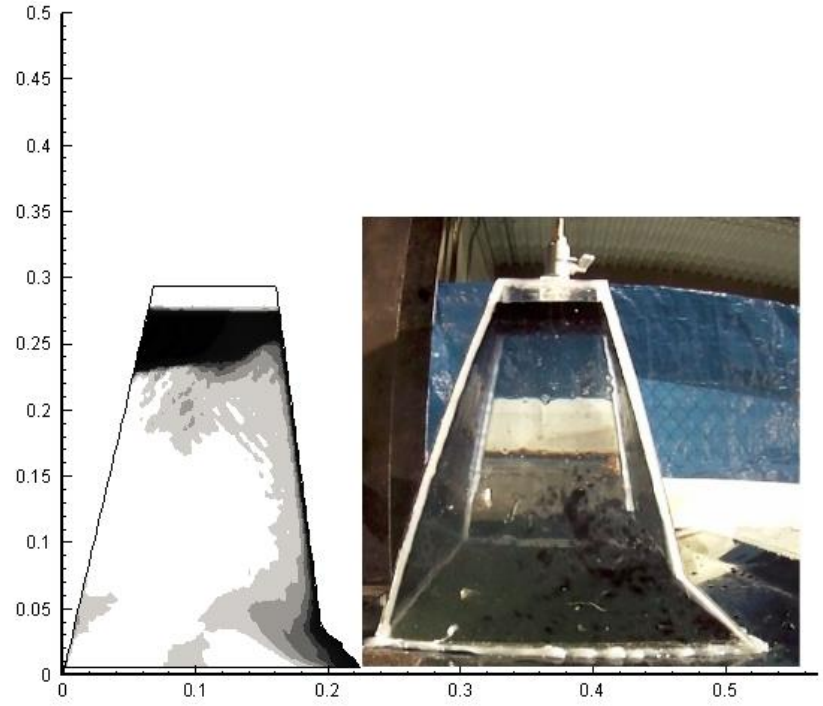

(3) Time instant=3.0 *s*

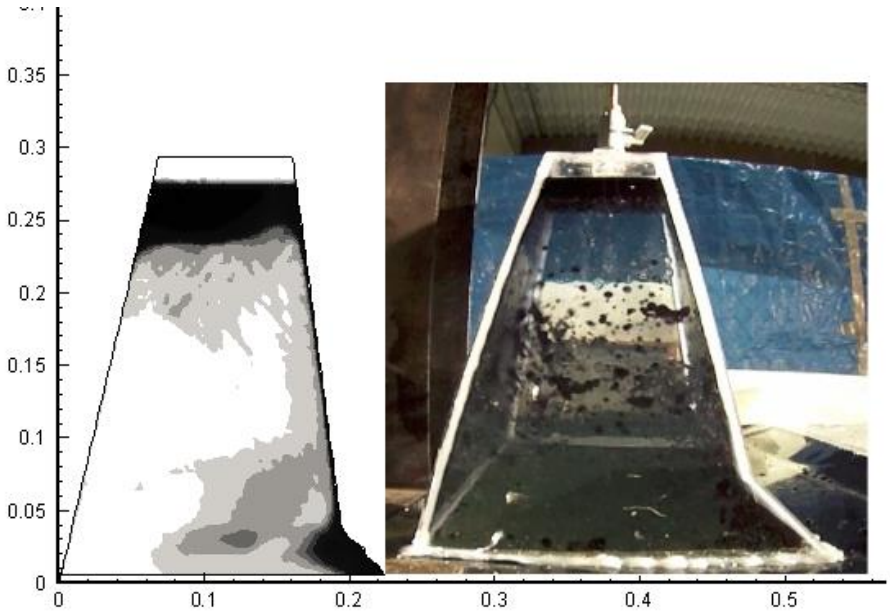

(4) Time instant=4.0 *s*

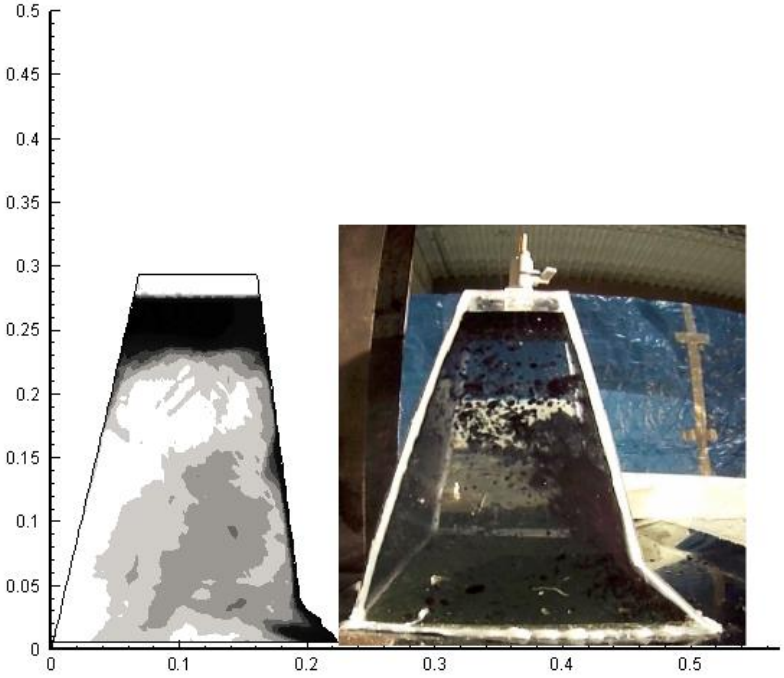

(5) Time instant=5.0 *s*

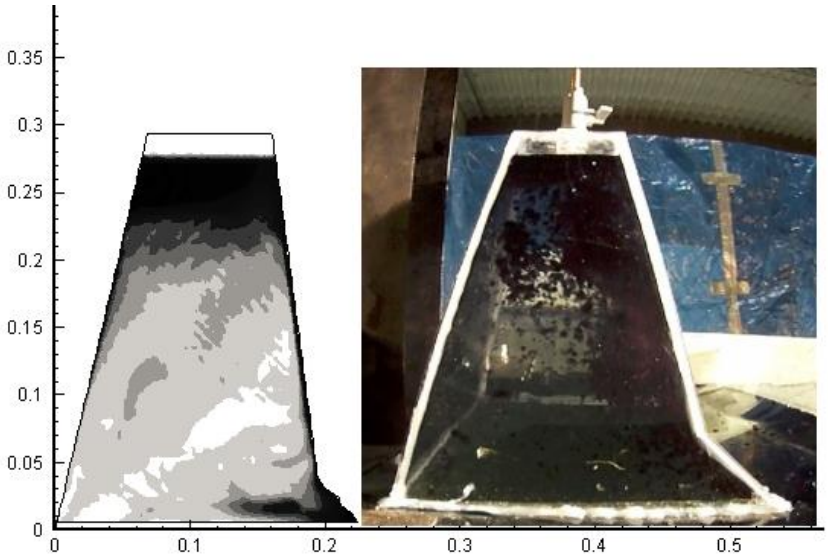

(6) Time instant=6. 0 *s*

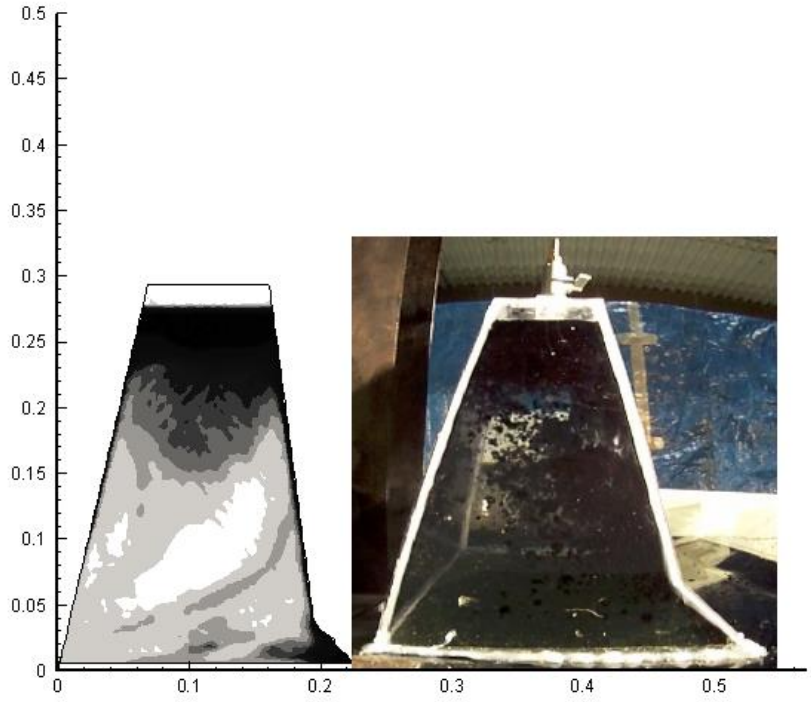

(7) Time instant=7. 0 *s*

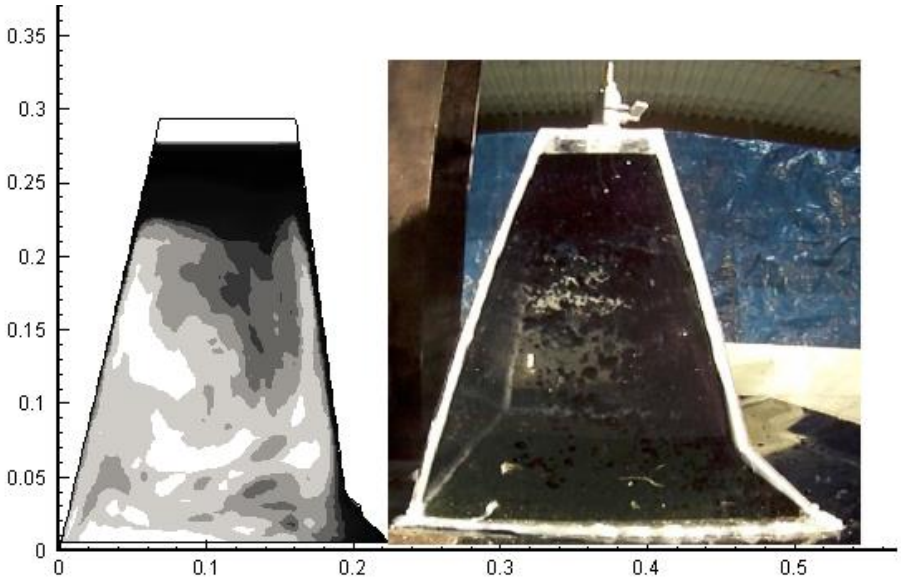

(8) Time instant=8. 0 *s*

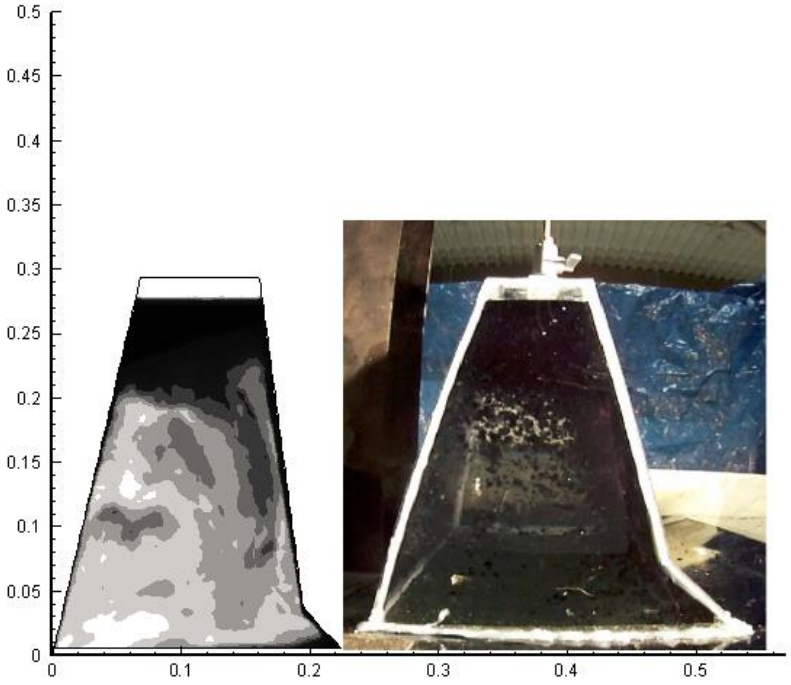

(9) Time instant=9.0 *s*

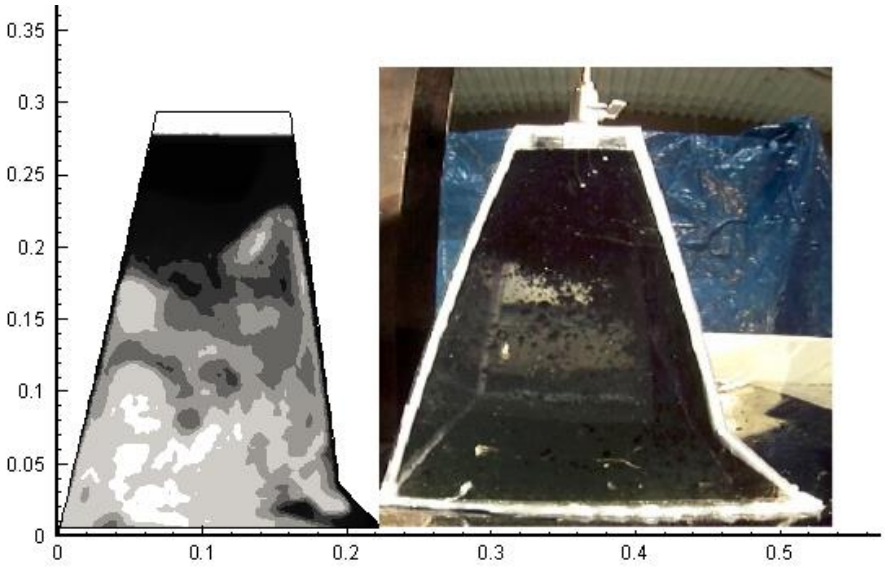

(10) Time instant=10.0 *s*

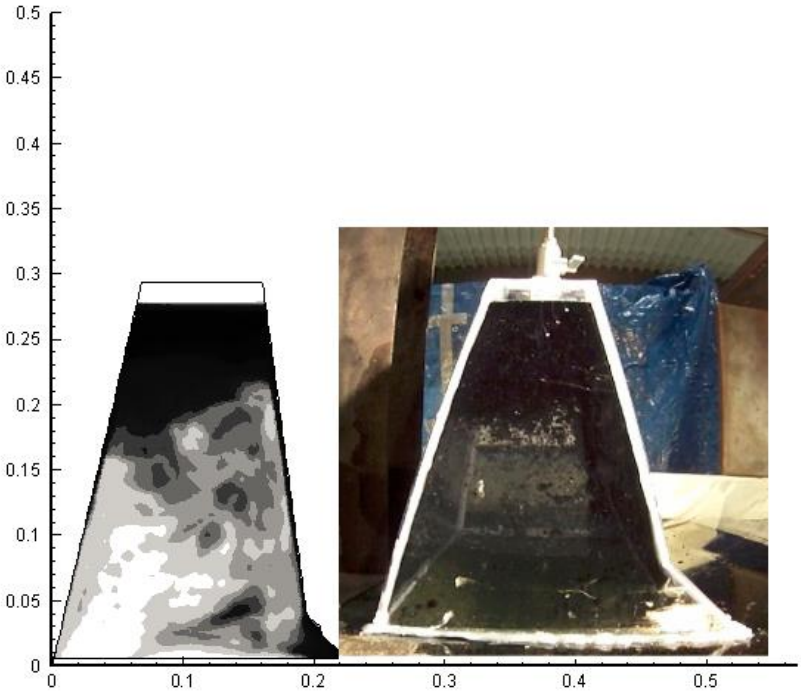

(11) Time instant=11.0 *s*

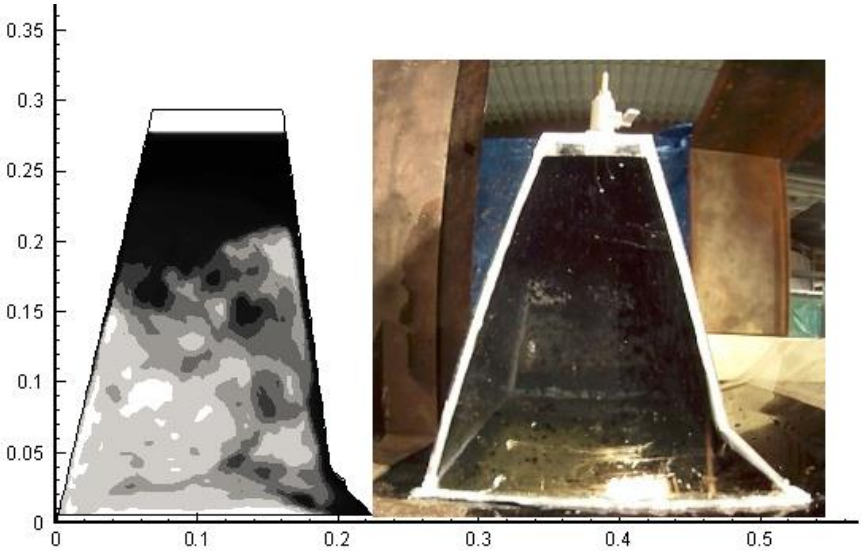

(12) Time instant=12.0 *s*

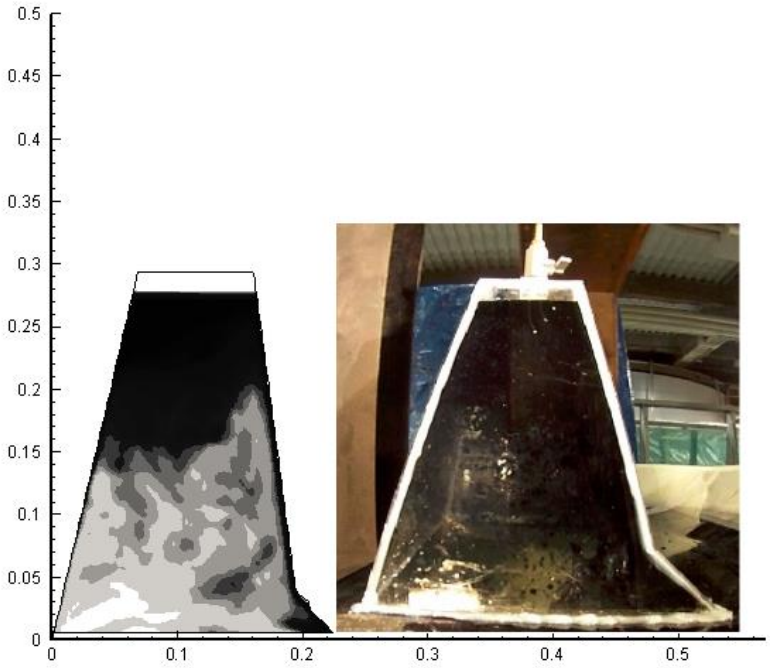

(13) Time instant=13.0 s

Figure 6.8 Comparison of oil flow patterns in the tower at speed of $0.216\ m/s$ (left:numerical, right: experimental)

Chapter 7

Conclusions

7.1 Summary

The process of oil recovery by the vacuum mechanism, involving multi-phase and multi-scale moving interfaces, has been simulated and evaluated using the Computational Fluid Dynamic method. The commercial CFD software, Star-CCM+, was adopted. The validation experiments were also carried out at Memorial University of Newfoundland. The simplified model was designed for the experimental purpose. The difference between experimental model and numerical model has been described. In addition, in order to verify the accuracy and reliability of Star-CCM+ applied in multi-phase-flow problem, a case involving multi-phase flows has been investigated. The results obtained from Star-CCM+ have been compared with the existing data, which showed that the CFD software is a reliable tool to handle three-phase-flow problems. The grid generation method, along with the convergence studies with various numbers of grids have been described. The model with 16.2 million grids was selected as the numerical model to compare with the experimental results. The comparisons of oil flow patterns obtained from numerical and experimental results have been presented. The initial numerical results agreed reasonably well with the experimental data using fine grids. The optimized simulations including both tower geometries and service speeds were also investigated. The numerical results from optimized geometries were compared with those from the original geometry. Since

the experiments with lower service speeds were also conducted, the comparisons of numerical and experimental results with lower service speeds have been showed.

The numerical results presented that the hydrodynamic performance of the oil skimmer model was successfully investigated. Based on the requirements from EST, the optimization have also been carried out. These improvements could seriously support the future design of the oil skimmer along with the field test in the open sea. However, comparing to the open sea condition, wave condition was not considered within this simulation model. The practical prototype was also more complicated than this simplified model used in the numerical simulation. There were more components and devices equiped with the prototype.

7.2 Future Work

The oil skimmer model used in the experiments is a simplified model due to ignoring the interaction between the skimming tower and the vessel hull. Since the skimming tower has two main ways to be optimized, the tower installed in the hull can be improved. The tower can be updated as a moving part that is robust for the installation corresponding to the optimized models in the numerical simulations. The connection equipment also can be updated to a light weight transferring component which allows the oil skimmer to press less on the water surface. The initial experiments were carried out in the trim tank with a length of 3.59 m. It took the skimmer 5.0 s, at $u = 0.527$ m/s, to travel from one end to the other end. If the towing test can be carried out in a towing tank

which is much longer than the trim tank, the oil flow motion and the oil skimming efficiency can also be observed more accurately, as the experimental data is much more elaborate. In order to obtain more accurate measurements of oil motion in the tower, the Particle Image Velocimetry (PIV) technique can be employed in the experiments.

The process of oil flow motion and hydrodynamic performance of the oil skimmer were numerically simulated using CFD software, Star-CCM+. One of the main reasons for the discrepancy between the experimental and numerical results could be inefficient grids distribution. The grids distribution might be able to improve and modify to have a better result. The computation time is affected by the total number of grids used in the simulation. The distribution of grids should be more efficient, and the distribution for the fluid interface must be particularly fine. In order to maintain the total number of grids for the simulation, the model size can be reduced. Then more grids can be applied in the oil layer, while the computation time will be kept at the same level.

The time step also can be modified by keeping the same value of the Courant number. Since the Courant number is required to be less than 1, it is varied when the time step changes. The numerical results with the optimized time step should agree with the experimental results more reasonably.

The discrepancies between the snapshots with higher speed and the snapshots with lower speed could be observed in Figure 5.7, which are probably due to the effectiveness of

incompressible air model. Since the snapshots from the numerical model with lower speed are matched better with the experimental results, the incompressible air model might be not working well in the model with $0.527\ m/s$. Therefore, different incompressible air models could be applied. In addition, other reasons to create the differences between the models with $0.527\ m/s$ and $0.216\ m/s$ will be investigated.

There are many ways to optimize the tower geometry in order to improve oil recovery efficiency. Lengthening the tower base can lead to a greater recovery efficiency since it allows oil to have sufficient time to flow into the tower. Increasing the angle of the rear tower surface also increases the recovery efficiency. In a further research plan, the volume of the skimming tower can be remained at the same value while modifying the tower base length or the rear surface angle. This study can be more specific to distinguish which optimized geometry leads to greater recovery efficiency.

The optimization studies have also confirmed that low service speeds lead to higher recovery efficiency. Future researches must include varied speeds, where the most optimized and most cost effective speed for the oil skimming rate will be identified. After optimizing the speed for the oil skimmer by numerical simulation, the validation tests should also be carried out.

The interaction between the catamaran hulls and the skimming tower will be investigated in future work. The hydrodynamic simulation for an oil skimmer installed with catamaran

should be conducted in following research. The seakeeping behavior in rough sea is essential for the practical applications. The process of oil recovery in waves shall also be studied numerically and experimentally. In addition, the numerical simulation of the oil skimmer working in a harsh environment, which includes skimming oil spills on ice, will be investigated.

Bibliography

Abascal, A.J., Castanedo, S., Medina, R. and Liste, M. (2010). "Analysis of The Reliability of a Statistical Oil Spill Response Model". *Marine Pollution Bulletin*, Vol. 60. No. 11, pp. 2099-2110.

Buist, I., McCourt, J., Potter, S., Ross, S. and Trudel, K. (1999). "In Situ Burning". *Pure Appl. Chem.*, Vol. 71, No. 1, pp. 43-65.

Buist I. (2003), "Window-of-Opportunity for In Situ Burning", *Spill Science and Technology Bulletin*, Vol.8, No.4, pp. 341-346.

CD-ADAPCO (2011). User Guide: Star-CCM+, version 6.04.014, *CD-ADAPCO*.

Chapman, H., Purnell, K., Law, R. and Kirby, M. (2007), "The Use of Chemical Dispersants to Combat Oil Spills at Sea: A review of practic and research needs in Europe", *Marine Pollution Bulletin*, Vol. 54, pp. 827-838.

Christodoulou, M., Turner, J. and Wilson, S. (1990), "A Model for the Low to Moderate Speed Performance of The Rotating Disk Skimmer", *Trans. ASME, Journal of Fluid Engineering*, Vol. 112, 476-480.

Clauss, G., Abu-Amro, M. and Kosleck, S. (2006). "Numerical and Experimental Optimization of a Seaway Independent Oil Skimming System - SOS". *International Offshore and Polar Engineering Conference*, San Francisco, California, pp.495-502.

Clauss, G. and Abu-Amro, M. (2007). "Hydrodynamic Optimization of an Ocean-Going Oil Recovery System in Harsh Seas". *Proceedings of OMAE 07, 26th International Conference on Offshore Mechanics and Arctic Engineering*, OMAE2007-29096.

Clauss, G., Habel, R., Vannahme, M. and Abu-Amro, M. (2002). "Development of Oil Skimming Vessels for High Seas". *10th International Congress of the International Maritime Association of the Mediterranean*, IMAM-2002, Crete, Greece.

Clauss, G. and Sprenger, F. (2009), "An Innovative Offshore Oil Skimming System for Operations in Harsh Seas". *13th Congress of International Association of Mediterranean*.

Clauss, G. and Abu-Amro, M. (2004). "Two-and Three-Phase Flow Computation for the Optimization of Oil Skimming Systems". *3rd International Symposium on Two-Phase Flow Modelling and Experimention*, 2004, Pisa, Italy.

Cochran, R. A. and Fraser, J. P. (1975). "Computer Simulation of Offshore Oil Spill Cleanup Operations". *Offshore Technology Conference*, OTC 2199, Dallas, Texas, US.

Cormack, D. (1983), "Response To Oil and Chemical Marine Pollution", *Applied Science Publisher*.

Daling, P., Singsaas, I., Reed, M. and Hansen, O. (2002) "Experiences in Dispersant Treatment of Experimental Oil Spills", *Spill Science and Technology Bulletin*, Vol. 7, Nos. 5-6, pp. 201-213.

Dewling, R. and McCarthy, L. (1980), "Chemical Treatment of Oil Spills", *Environmental International*, Vol. 3, pp. 155-162.

Diemand, R. and Francis, K. (2011), "Dispersants for Crude Oil Spills: Dispersant Behavior Studies", *Worcester Polytechnic Institute*.

Evans, D., Mulholland, G., Baum, H., Walton, W. and McGrattan, K. (2001), "In Situ Burnign of Oil Spills", *Journal of Research of the National Institute of Standards and Technology*, Vol. 106, No. 1, pp. 231-278.

Fraser, J.P. and Clark, L.M.C. (1984). "SOCK Skimmer Performance and Field Tests". *Journal of Petroleum Technology*, Vol. 36, No.3, pp. 451-456.

Goodman, R., Brown, H., An, C. and Rowe, R. (1996), "Dynamic Modelling of Oil Boom Failure Using Computational Fluid Dynamics", *Spill Science and Technoly Bulletin*, Vol. 3, No.4, pp. 213-216.

Graham, P. (2010), "Deep Sea Oil Spill Cleanup Techniques: Applicability, Trade-offs and Advantages", *Discovery Guides2010, ProQuest*, pp.1-15.

Hammoud, A. (2006), "Enhanced Oil Spill Recovery Rate Using Weir Skimmer", *5th International Conference on Oil Spill in the Mediterranean Sea*.

Hirt, C. W. and Nichols, B. D. (1981). "Volume of Fluid (VOF) Method for the Dynamics of Free Boundaries". *Journal of Computational Physics*, Vol. 39 , No.1, pp. 201-225.

Hyman, J. (1984). "Numerical Methods for Tracking Interfaces". *Physica 12D, North-Holland Physics Publishing Division*, pp. 396-407.

Kawano, S. and Hashimoto, H. (1992), "Drag Coefficient of a Spherical Encapsulated Liquid Drop", *JSME International Journal*, Series II, Vol. 35, No.2, pp. 151-157.

Kawano, S., Shirai, A. and Nagasaka, S. (2007), "Deformations of Thin Liquid Spherical Shells in Liquid-Liquid-Gas Systems", *Physics of Fluids* 19, 012105 (2007), DOI: 10. 1063/1.2429070.

Kawano, S., Hashimoto, H. Ihara, A. and Shin, K. (1996), "Sequential Production of mm-sized Spherical Shells in Liquid-Liquid-Gas Systems", *Trans. ASME, J. Fluid Eng.*, 118, 614.

Leibovich, S. and Cornell, U. (1977). "Hydrodynamic Problems in Oil-Spill Control and Removal". *Journal of Petroleum Technology*, Vol. 29, No. 3, pp. 3111-324.

Lemesle, P., Kakalis, N., Fritsch, D. and Turan, O. (2006). "Design of Monohull EUMOP Units to Clean Oil Spills". *Small Craft Conference*, Bodrum, Turkey.

Lessard, R. and Demarco, G. (2000), "The Significance of Oil Spill Dispersants", *Spill Science and Technology Bulletin,* Vol. 6, No. 1, pp. 59-68.

Menter, F. R. (1994). "Two-Equation Eddy-Viscosity Turbulence Models for Engineering Applications". *AIAA Journal,* Vol. 32, No. 8, pp.1598-1605.

Moxness, V. W., Gaseidnes, K. and Asheim, H. (2011). "Skimmer Capacity for Viscous Oil". *SPE Journal,* Vol. 16, pp. 155-161.

Mullin, J., and Champ, M. (2003), "Introduction/Overview to In Situ Burning of Oil Spills", *Spill Science and Technology Bulletin*, Vol. 8, No. 4, pp. 323-330.

Muttin, F. (2008). "Structural Analysis of Oil-Spill Containment Booms in Coastal and Estuary Waters". *Applied Ocean Research 30,* pp. 107-112.

Najar, A. and Turner, J. (1999), "Enhanced Oil Recovery Using the Rotating Disk Skimmer", *Journal of Process Mechanical Engineering*, Part E, Vol. 214, pp. 271-282.

Navier, C. L. (1822). "Memoire Sur Les Lois du Mouvement des Fluides". *Mem. Acad. Sci. Inst.* France, Vol. 6, pp. 389-440.

Ni, S., Qiu, W., and Zhang, A. and Prior, D. (2013). "Hydrodynamic Simulation and Optimization of an Oil Skimmer". *Proceedings of the ASME 2013, 32nd International Conference on Ocean, Offshore and Arctic Engineering*, OMAE2013-11499.

Noh, W. F. and Woodward, P. (1976). "SLIC (Simple Line Interface Calculation)". *Proceedings of the Fifth International Conference on Numerical Methods in Fluid Dynamics*, Vol. 59, pp. 330-340.

Nordvik, B., Champ, A. and Bitting, K. (2003), “Estimating Time Windows for Burning Oil at Sea: Processes and Factors”, *Spill Science and Technology Bulletin*, Vol. 8, No.4, pp. 347-359.

Nordvik, A., Simmons, J. and Bitting, K. (1996), “Oil and Water Separation in Marine Oil Spill Clean-up Operations”, *Spill Science and Technology Bulletin*, Vol. 3, No. 3, pp. 107-122.

Reed, M., Daling, P., Lewis, A., Ditlevsen, M., Brors, B., Clark, J. and Aurand, D. (2004), “Modeling of Dispersant Application to Oil Spills in Shallow Coastal Waters”, *Environmental Modelling and Software*, Vol. 19, pp. 681-690.

Reynolds, O. (1895). “On the Dynamical Theory of Incompressible Viscous Fluids and the Determination of the Criterion”. *Philosophical Transactions of the Royal Society of London*. A, Vol. 186, pp. 123-164.

Stokes, G. G. (1849), “On the Theories of the Internal Friction of Fluids in Motion, and of the Equilibrium and Motion of Elastic Solids”. *Transactions of the Cambridge Philosophical Society*, Vol. 8, pp. 287-319.

Thomas, G. (1977), “Oil Recovery Devices”, *Technical Memorandum*, No. 132 083, B. P. Research Centre, Sunbury-On-Tham.

Ubbink, O. (1997). “Numerical Prediction of Two Fluid Systems with Sharp Interfaces”. *Department of Mechanical Engineering*, Imperial College of Science, Technology and Medicine, London, Engla

Victoria B. and A. Keller, A. (2006). “Improved Mechanical Oil Spill Recovery Using an Optimized Geometry for the Skimmer Surface”. *Environ. Sci. Technol.*, Vol. 40, pp. 7814-7918.

Violeau, D., Buvat, C., Abed-Meraim, K. and de Nanteuil, E. (2007), “Numerical Modelling of Boom and Oil Spill with SPH”, *Coastal Engineering*, Vol. 54, pp. 895-913.

Wong, K. and Stewart, H. (2003), “Oil Spill Boom Design for Waves”, *Spill Science and Technology Bulletin*, Vol. 8, Nos. 5-6, pp. 543-548.

Wong, K. and Barin, E. (2003), “Oil Spill Containment by a Flexible Boom System”, *Spill Science and Technology Bulletin*, Vol. 8, Nos. 5-6, pp. 509-520.

Yang, X. and Liu, M. (2013), “Numerical Modeling of Oil Spill Ccontainment by Boom Using SPH”, *Science China-Physics Mechanics Astronomy*, Vol. 56, pp. 315-321, doi: 10.1007/s11433-012-4980-6.